

Review

Progress in the Photoreforming of Carboxylic Acids for Hydrogen Production

Anita Samage¹, Pooja Gupta², Mahaveer A. Halakarni¹, Sanna Kotrappanavar Nataraj^{1,*}
and Apurba Sinhamahapatra^{2,*}

¹ Centre for Nano and Material Sciences, Jain Global Campus, Jain University, Bengaluru 562112, Karnataka, India; samageanita1008@gmail.com (A.S.); a.mahaveer@jainuniversity.ac.in (M.A.H.)

² Department of Chemical Engineering, Indian Institute of Technology (Indian School of Mines), Dhanbad 826004, Jharkhand, India; pooja.guupptaa@gmail.com

* Correspondence: sk.nataraj@jainuniversity.ac.in or sknata@gmail.com (S.K.N.); apurba@iitism.ac.in or apurbasmp03@gmail.com (A.S.)

Abstract: Photoreforming is a process that connects the redox capability of photocatalysts upon light illumination to simultaneously drive the reduction of protons into hydrogen and the oxidation of organic substrates. Over the past few decades, researchers have devoted substantial efforts to enhancing the photocatalytic activity of the catalyst in hydrogen production. Currently, the realization of the potential of photocatalysts for simultaneous hydrogen production with value-added organics has motivated the research field to use the photo-oxidation path. As a distinct benefit, the less energetically demanding organic reforming is highly favorable compared to the slow kinetics of oxygen evolution, negating the need for expensive and/or harmful hole scavengers. Photocatalyst modifications, such as secondary component deposition, doping, defect, phase and morphology engineering, have been the main strategies adopted to tune the photo-oxidation pathways and oxidation products. The effect of the reaction parameters, including temperature, pH, reactant concentration and promising reactor strategies, can further enhance selectivity toward desired outcomes. This review provides a critical overview of photocatalysts in hydrogen production, including chemical reactions occurring with semiconductors and co-catalysts. The use of various oxygenates as sacrificial agents for hydrogen production is outlined in view of the transition of fossil fuels to clean energy. This review mainly focuses on recent development in the photoreforming of carboxylic acids, produced from the primary source, lignocellulose, through pyrolysis. The photo-oxidation of different carboxylic acids, e.g., formic acid, acetic acid and lactic acid, over different photocatalysts for hydrogen production is reviewed.

Keywords: photoreforming; solar; hydrogen; carboxylic acids



Citation: Samage, A.; Gupta, P.; Halakarni, M.A.; Nataraj, S.K.; Sinhamahapatra, A. Progress in the Photoreforming of Carboxylic Acids for Hydrogen Production. *Photochem* **2022**, *2*, 580–608. <https://doi.org/10.3390/photochem2030040>

Academic Editor: Vincenzo Vaiano

Received: 22 June 2022

Accepted: 22 July 2022

Published: 29 July 2022

Publisher's Note: MDPI stays neutral with regard to jurisdictional claims in published maps and institutional affiliations.

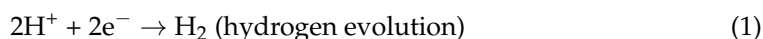


Copyright: © 2022 by the authors. Licensee MDPI, Basel, Switzerland. This article is an open access article distributed under the terms and conditions of the Creative Commons Attribution (CC BY) license (<https://creativecommons.org/licenses/by/4.0/>).

1. Introduction

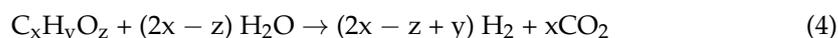
One of the major technological challenges in today's world is obtaining a sustainable clean energy source. Over the past few decades, the world's energy consumption has increased exponentially due to overpopulation, overconsumption and aged energy storage systems, leading to the high consumption of non-renewable fossil fuels [1]. The more extensive use of fossil fuels results in elevated concentrations of atmospheric greenhouse gases; for example, carbon dioxide affects the environment of the total globe, which causes deviation and threatens biodiversity [2]. To overcome these major problems of the present earth, breakthrough solutions and innovative energy production technologies depending on renewable resources are required to compensate for carbon debt. As the world is traversing toward carbonless and renewable energy sources, hydrogen (H₂) is becoming an increasingly powerful medium as a versatile energy carrier, enabling a globe with a

zero-emission economy, and it has higher energy density than the conventional fossil-fuel-based sources [3]. H₂ is a lightweight energy carrier, which can be easily converted into electricity and drinkable water as a byproduct via fuel cell technology. Therefore, H₂ can prevent emissions from the transport and energy sectors, making the system emission-free. Moreover, it has been used in the production of chemicals such as ammonia (through Haber's process), urea and in the manufacturing of steel. Here, in these processes, used H₂ was derived from the gasification of coal [4], water gas shift reactions [5] and methane reforming [6]. These traditional hydrogen production methods have carbon dioxide footprints and are not renewable, environment-friendly and sustainable procedures. Most of the methods mentioned above require high temperatures, pressure conditions and the use of an external bias or non-renewable fossil fuels. Therefore, there is a need to produce hydrogen from renewable, sustainable and environmentally benign sources of green origin, which should be cost-effective [7]. Therefore, industries and transport sections can use hydrogen fuel efficiently and meet our energy demands for energy storage resolutions. As a result, moving from non-renewable fossil fuels to the hydrogen economy requires effective methodologies to allow clean, sustainable and cost-effective production and H₂ storage systems. Various types of technologies have been projected so far, such as chemical, thermal, electrochemical, photo electrolytic and photocatalytic processes. These methods make use of water, biomass waste and fossil fuels as feed stocks for the generation of hydrogen [8]. In recent trends, solar-light-assisted methods utilizing solar radiations and water/renewable precursors have advantages and have gained noteworthy attraction over the past few decades. Recent investigation has predicted that H₂ production using solar-light-supported methods are more advantageous than the traditional technologies, which are based non-renewable energy sources. The photocatalytic water-splitting reactions takes place via two half reactions (i.e., proton reduction and the transferring of four electrons for the oxidation of water) [9].



Subsequently, in 1972 Honda and Fusishima described the effective use of visible light radiation in an electrochemical system to decompose water into O₂ and H₂ using TiO₂ as a photocatalyst [10]. Various types of catalysts are used in the water's electrocatalytic and photocatalytic H₂ production. The most demanding and exciting process is the photocatalytic production of H₂ from water at ambient temperature and pressure, which converts and stores solar energy in the form of chemical energy [11]. Even though photocatalytic H₂ production has neutral carbon footprints and renewable energy sources (secondary light sources or direct sunlight), it has encountered some challenges. Initially, it lacked advanced photocatalysts, which have more thermodynamic barriers for overall water splitting, which results in higher energy requirements with respect to intense light sources and requires a suitable sacrificial agent [12,13]. Various methods have been proposed to enhance the photocatalytic efficiency of catalysts in the form of structural modification, tuned morphology, the addition of cocatalysts, etc., which are mainly implemented for better charge generation and transfer efficiency. However, practical efforts are still required for the further enhancement of quantum efficiency and high yield production [14]. In addition, geographic segregation and the scarcity of clean water for conventional water splitting has led to challenging interests in using portable water sources. Therefore, to overcome these aforementioned challenges, photocatalytic H₂ production with simultaneous organic reforming (photoreforming) is an efficient alternative method. The photoreforming reaction occurs via the oxidation of organic molecules [15]. This organic support acts as a proton

source. Therefore, it is a coupling reaction of substrate oxidation and proton reduction. The primary reaction is as shown in the following equation: [16,17].



The advantages of the photoreforming process over traditional photocatalytic water splitting include: the backwards reaction of O_2 and H_2 during photocatalytic water splitting can be prevented; organic precursors or biomass are employed, which is a less energy-consuming process to replace kinetically sluggish oxygen evolution reactions by allowing higher efficiency in H_2 evolution; and waste/biomass can be converted into valuable products or organic compounds. The use of organics in photocatalytic H_2 production gives an alternative catalytic path; heat-absorbing organic molecules replace the vast energy required for water oxidation with organic molecule oxidation, which has lesser Gibbs free energy and leads to a lower thermodynamic energy barrier [18]. In this process, chemical feedstocks can be used from industries (food and beverages), agricultural waste and organics to simplify the reaction. Researchers have mainly focused on the photocatalytic oxidation of organics and biomass degradation during the last few decades, although various mechanistic depth investigations have been undertaken [19]. Most of the works concentrate exclusively on enhancing H_2 production efficiency or increasing the selectivity in the oxidation process. The coupling of H_2 production and selective organic oxidation into valuable products remains incoherent. Most of the studies have demonstrated the mechanism of the formation of H_2 with increased efficiency without considering the oxidation mechanism. Understanding the oxidation and reduction mechanism in the whole photoreforming process is vital to realizing the potential of selective photoreforming in producing the H_2 and individual organic molecules. In this context, the implementation of photoreforming process on an industrial scale and the selectivity of organic oxidation play an essential role in the formation of specific valuable organic products. For example, the oxidation of glycerol can produce glyceraldehyde, glyceric acid and glycolic acid [20] while preventing the generation of waste products results in photoreforming, which is the only process producing H_2 with waste management [21]. The reaction selectivity and efficiency can be obtained by rationalizing catalyst material and reaction [22] media. This method allows a great opportunity to synthesize a particular organic molecule with simultaneous reductions in dependence on non-renewable fuels.

The present review describes the importance of photocatalysis in hydrogen formation with the support of literature reports, including review articles. The photoreforming of carboxylic acids into hydrogen with byproducts is expressed systematically, and the effect of catalytic materials, cocatalysts and sacrificial agents is reviewed thoroughly. A brief introduction to elementary steps in the photoreforming of carboxylic acids has been given. The impact of using organic acids on the production of H_2 is discussed critically. Considerations of recent developments in novel synthetic strategies and activity toward the photoreforming of acids are discussed with organic/inorganic photocatalysts.

2. Details of the Photoreforming Process

The photocatalytic reactions occur through a chain of events in the presence of semi-conducting materials. The photocatalytic reactions in different conditions are summarized in Figure 1 for water splitting and photoreforming reactions. In a photoreforming reaction, the initial crucial step is light absorption and the formation of charge carriers, such as electrons and hole pairs (e^-/h^+). This charge carrier pair formation should occur upon irradiating the solar radiation on semiconducting materials using visible region energy, and to cause the reaction, the catalytic materials should be exposed to higher-energy radiation than its band gap energy. The electrons (e^-) from the valence band (VB) are excited to the conduction band (CB) by leaving holes (h^+) behind [23]. The photogenerated charge carriers follow various pathways, such as the recombination of charge carriers at bulk/surface of catalyst leads to decrease in photocatalytic activity. Once these charge carriers are separated and transferred to the catalyst surface, they can reduce and oxidize the reactants.

The formation and realization of a specific reaction are related to the band structures of semiconducting materials. The capacity of e^- and h^+ towards reduction and oxidation reactions can be defined using the edge potentials of CB and VB [15].

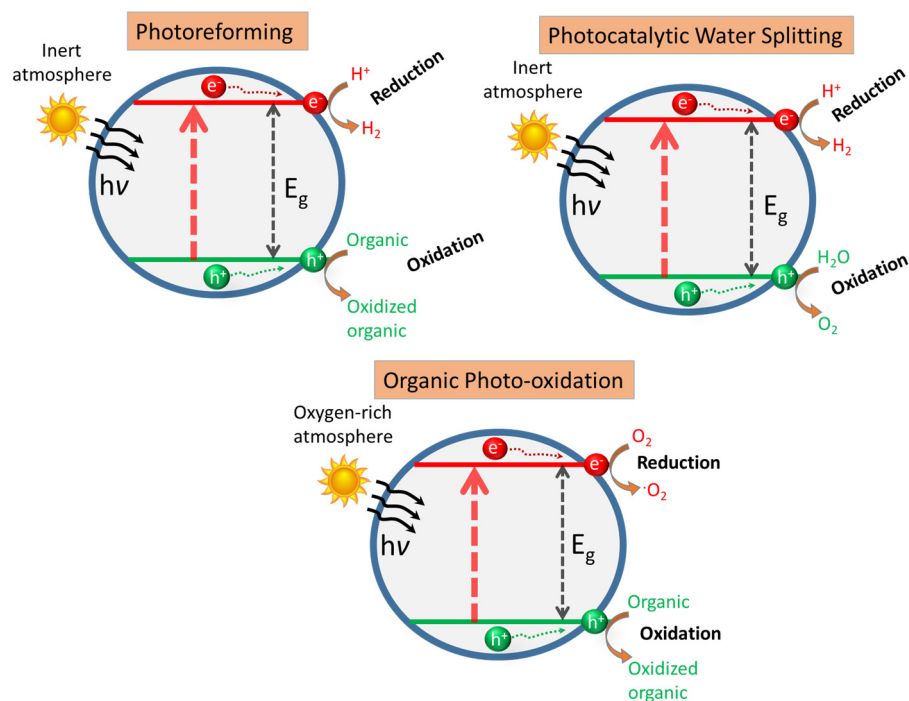


Figure 1. Mechanism involved in photoreforming, photocatalytic water splitting and organic photo-oxidation [15].

In the photocatalytic production of H_2 , the bottom of the VB should be more negative than the H^+/H_2 redox couple (0 V vs. NHE) at a neutral pH. In a water-splitting reaction for the oxidation of water, the top of the VB should be more positive than the O_2/H_2O oxidation potential of 1.23 vs. NHE at a neutral pH [24]. Therefore, theoretically, the minimal value for the oxidation of water is 1.23 V vs. NHE at a neutral pH. In practice, this value increases to 2–2.4 eV because of the kinetic over-potential and energy loss during a reaction. With respect to thermodynamical parameters, water splitting requires higher positive Gibbs free energy ($\Delta G_0 = +237.2$ kJ/mol) [25]. This oxidation reaction is an endothermic half-reaction; however, the overall reaction provides H^+ and e^- for the reduction reaction to produce H_2 . The mechanism involved in photoreforming, photocatalytic water splitting and photo-organic oxidation is displayed in Figure 1. In recent years, the demand for oxygen evolution reaction has been a bottleneck for the water-splitting reaction. Subsequently, there are narrow band gap (E_g) materials, which can catalyze both the oxidation and reduction reactions. In particular, working at a neutral pH is more challenging with respect to thermodynamics due to the lower availability of protons. Usually, in order to assess the capacity of photocatalysts, sacrificial agents are used to control the productivity towards one of the two half-reactions. However, the catalytic activity of the material towards one of the two half-reactions of water splitting is not necessary to be active for overall water splitting. In the photoreforming process, the oxidation potential is 0.08 V vs. NHE using organic substrates for scavenging h^+ more productively, which consumes h^+ rapidly by preventing charge recombination. Moreover, it can serve as a proton source [26]. With respect to thermodynamic studies, the photoreforming process is less challenging than water splitting, and it also reduces the reversible combination of H_2 and O_2 . Therefore, the photoreforming process can be considered realistic; when the scavenging agents are abundant and easily accessible, sustainable and cost effective [15]. Various types of semiconducting materials have been established and utilized in photo-

assisted H₂ production processes. Despite noteworthy efforts, efficiency and promising results are far from commercialization. Among all the reported photocatalytic materials, TiO₂ is most widely used because of its non-toxicity, chemical stability and low cost. In addition, TiO₂ displays a high rate of recombination, and it has wide band gap of around 3.2 eV for anatase, which absorbs the UV light range. This results in low efficient materials towards photocatalysts because solar energy has only 3 to 4% of UV radiation [27]. Generally, an ideal photocatalyst should have the following properties: it should be efficient towards harvesting sun light and generating the redox charge carriers, it should have stability under working conditions and it should be more economical.

Along with this, some technical challenges are designing the appropriate semiconductors with effective charge carrier separation, a high rate of diffusion of the produced charge carriers and their movement towards the active centers of the surface, the appropriate arrangement of edge potentials in the CB and VB for the desired reactions, exposed reaction sites and easy preparation of catalytic materials without using infrequent materials [28]. This results in the enhancement of the efficiency of the catalyst, mainly depending on engineering materials, which should lead towards improving the significant parameters. The band gap, band positions and redox potentials of various types of photocatalytic materials are described in Figure 2.

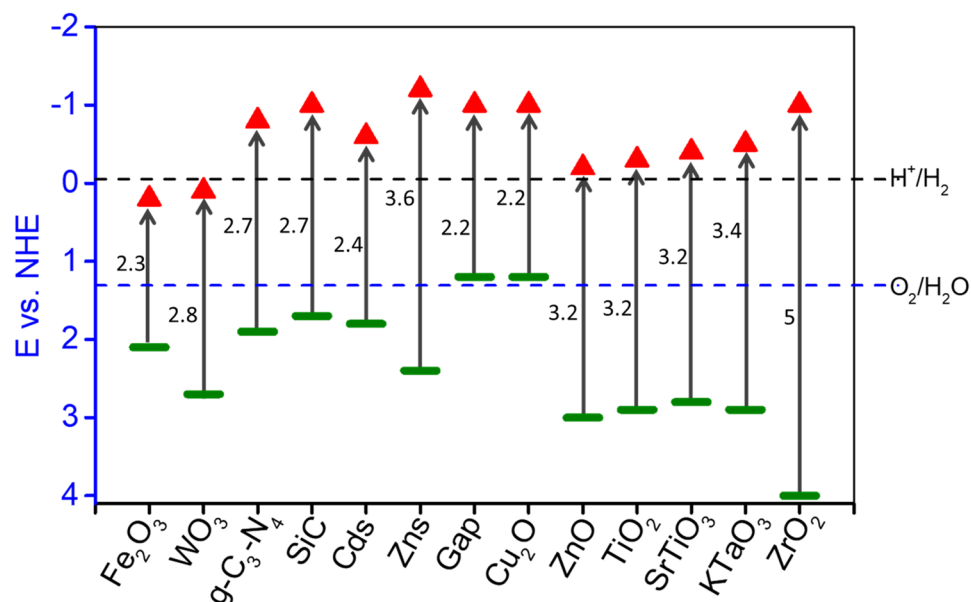
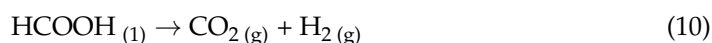
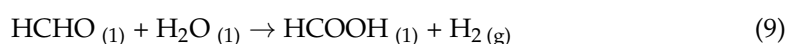
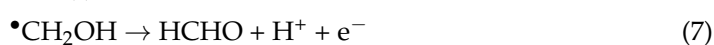
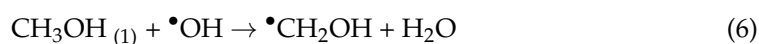


Figure 2. Presentation of band gaps and positions of various photocatalysts as well as selected redox potentials [27].

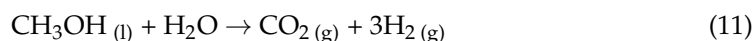
3. Types of Organics (Oxygenates) in the Photoreforming Process for H₂ Production

The photo-formation of H₂ from different organic molecules in the existence of semi-conducting materials was first introduced by Kawai and Sakata in the initial stage of the 1980s. Various organic molecules are used in photocatalytic reactions, i.e., sugars and carboxylic acids over RuO₂/TiO₂ [29] and Pt/TiO₂ [30], respectively. In the last several decades, various sacrificial agents have been used in the production of hydrogen, for example, glycerol, glucose, ethanol [31], methanol [32], carboxylic acids [33], amino acids, biomass [34], fossil fuels, etc. Earlier reports suggest that the photo formation of H₂ from water using hydrocarbons as a sacrificial mediator has recently attracted considerable attention. Research mainly focuses on the improvement of the efficiency of catalyst materials and also on the technological aspects and behavior of sacrificial agents towards efficiency. Various organic molecules have been demonstrated previously. Sacrificial agent/hole scavengers play a crucial role in the photoproduction of H₂. The need for refilling sacrificial reagents in order to sustain high rates of reaction precludes their effective use for large-scale

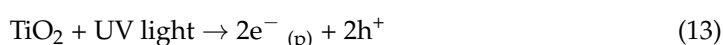
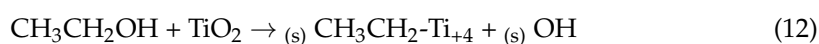
and continuous production of H₂. Alternatively, sacrificial reagents can be used to assess the photocatalytic efficiency of H₂ evolution [35]. Mainly, the fundamental mechanism associated with hydrogen-containing sacrificial reagents is whether these reagents simply serve as hole scavengers, which means that the species rapidly react with holes diminish their amount and thus stop their recombination with photogenerated electrons, leading towards higher efficiency. In addition, sacrificial agents may contribute their hydrogen atoms to produce H₂ [36]. The most commonly used sacrificial agent is methanol due to its simplicity, its high amount of hydrogen, its understandable reaction mechanism and its capability of capturing h⁺. Earlier, methanol was used as an ideal feed stock in photoreforming [37]. The photochemical reaction of methanol and its degradation products are described as follows:

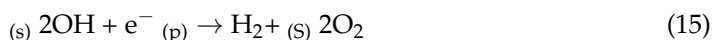


Overall reaction:



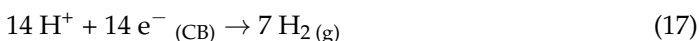
For the first time, H₂ production was performed using methanol by Kawai and Sakata in the 1980s. The proposed plausible mechanism predicted the formation of formaldehyde then into formic acid and further decomposing into H₂ and carbon dioxide [29]. Li et al. reported the efficiency of hydrogen production in the presence of various sacrificial agents, thus showing improvement in photocatalytic activity by reducing the C/OH ratio. In addition, the scavengers react with hydroxyl radicals, enhancing the activity with the simplest molecule structure [38]. The systematic investigation was conducted using functionalized TiO₂ with various noble and earth-abundant elements [39]. Recent research reports that copper-impregnated TiO₂ [40], niobium pentoxides [41] MoS₂/TiO₂ [42] and H-Doped TiO_{2-x} (H:TiO_{2-x}) [43] are used in the photoreforming of methanol into hydrogen. Paramasivan et al. reported in situ simultaneous copper-deposition-enhanced photocatalytic hydrogen production from aqueous methanol solutions using ZnO as a photocatalyst. Hydrogen production was increased to be 130 times better than bare ZnO, and Cu-deposited Zn responded to visible light for hydrogen formation. The photogenerated holes attack methanol to form formaldehyde, which is further oxidized with OH radicals, and the holes produce formic acid. The photogenerated electrons reduce copper ions into a metallic copper cluster, which stores electrons. The electron sink role of Cu in ZnO enhances the separation of photogenerated electron-hole pairs and thus prevents the recombination of electron-hole pairs [44]. The schematic mechanism is shown in Figure 3a. Various transition metals as photocatalytic materials are used in hydrogen generation [45]. Furthermore, ethanol was investigated as a sacrificial agent in photoreforming H₂ formation, because it can be obtained from biomass (cellulose and lignocellulose). Ethanol photoreforming includes the production of acetic acid and acetaldehyde, which is associated with the reduction of H⁺. There are other reaction pathways, including the direct reaction of h⁺ with ethanol that produces acetaldehyde by forming ethoxide ions on the catalyst surface and the oxidation of ethanol through OH[•] formation [46]. The produced byproducts are mainly acetaldehyde and CO, CO₂, C₂H₄ and C₂H₆ in different amounts, as described in the following reaction [47,48]:



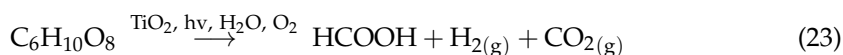
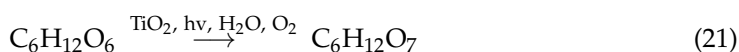
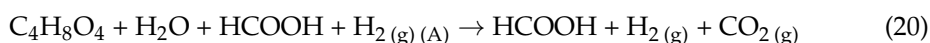
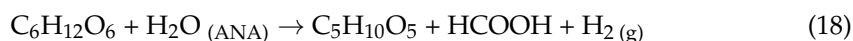


Here, (s) represents the surface of the photocatalyst, and (p) represents photoexcited electrons.

The ethanol oxidation produced H₂ with 50% quantum efficiency using Pt/TiO₂ catalyst. Recently, ethanol oxidation was carried out on Au and TiO₂ (Figure 3b) [49] and in-situ photo-deposited Ni cocatalysts carbon nitride with cyanamide functionalities to enhance the activity and selectivity. The cyanamide functionalities mainly promote hole scavenging for ethanol oxidation [50]. Glycerol is a byproduct of the biodiesel and soap industry, which produces a large amount of 10 wt%. As it has less demand in the market, it is considered waste and is used in H₂ production in photoreforming. As glycerol is a hydrogen source and an e⁻ releaser, various catalysts, such as engineered TiO₂-based photocatalysts, are used. The photoreforming of glycerol produces acids, ketones and alcohols, as described in the following Equations (16) and (17) [51].



Further research continued to use various catalysts, such as 2D Au/TiO₂ [52], Pt/TiO₂-Nb₂O₅ [53] and Au-NPs embedded in WO₃/TiO₂ (Figure 3c) [54] in recent studies for water and glycerol mixture reforming into hydrogen. Furthermore, polysaccharides are gaining more attention in the photoreforming process due to their thermodynamically acceptable nature with negative Gibbs free energy. Glucose can mainly be extracted from cellulose hydrolysis, and a higher amount of sugar is found in wastewater from food processing industries. Therefore, various photocatalysts are checked to obtain H₂. The glucose-reforming mechanism was initially investigated in 1983 by Michael R. St. Jhon et al. on a platinized TiO₂ surface [55]. It was thoroughly studied using D-glucose, and they proposed a detailed reaction mechanism in glucose reforming, as summarized in the following reaction Equations (18)–(23) [56,57].



Here, ANA represents the anaerobic condition, and A represents the aerobic condition.

In recent studies, graphene dots functionalized with Pt cocatalysts were used in the photo reforming of cellulose in an alkaline medium, which forms glucose in the first step, and continuous H₂ production for 6 days was achieved, as displayed in Figure 3d [58]. The photoreforming of protein molecules, amines and amino acids was studied using glycine and glutamic acid, which are the most common in living organisms [59]. The irradiation of these amino acids and proteins in the presence of Pt/TiO₂ results in the production of H₂ and CO₂ in neutral water and H₂ and NH₃ in alkaline. Both NH₃ in neutral solutions and CO₂ in basic solutions were absorbed in water and not released in the gas phase [60]; moreover, CO₂ can be reduced in valuable fuels [61]. As discussed above, along with photo conversion of biomass-derived compounds, the employment of raw biomass materials for photoreforming was also explored, in which photo generated holes oxidizes biomass substrates and electrons drove photoexcitation. However, the selective photo-transformation

of unprocessed biomass into valuable products is a still difficult task. Very few efforts have been made to obtain the selective chemical transformation of unprocessed biomass into useful products. Initially, Greenbaum et al. used ZnO as a catalyst material for directly converting biomass into hydrocarbons and O_2 under UV-visible light radiation [62]. In addition, Wu et al. reported an efficient approach toward producing functionalized aromatic compounds from lignin with a lignocellulosic biomass over CdS quantum dots. The mechanistic investigation indicated that both photoinduced electrons and holes are involved in the cleavage of the β -O-4 linkage of lignin via the EHCO mechanism. Most of the efforts are dedicated to sustainable hydrogen production by combining the simultaneous photo-oxidation of an aqueous biomass and the photocatalytic evolution of hydrogen at room temperature and atmospheric pressure [63]. Recently, an enhancement in the rate of H_2 evolution was achieved in the photoreforming of lignocellulose with the irradiation of visible light. The high rate of H_2 production was evidenced by the photoreforming of purified and raw lignocellulose over nanostructured carbon nitride under benign conditions without any toxic chemicals. Andrea Speltini et al. used oxidized g- C_3N_4 for the evolution of hydrogen assisted by an aqueous biomass in the presence of simulated solar radiation and compared the performance with that of P25- TiO_2 [64]. Furthermore, Qiong Liu et al. evolved hydrogen by the photoreforming of biomass by using a functionalized terminal amino group in carbon nitride by in situ C-N coupling [65]. The photoreforming of the biomass into hydrogen and valuable products is carried out on an earth-abundant metal oxide, such as a Co/CoO hybrid structure with an excellent rate of 12 mmol/g/h, which is higher than the commercial catalyst [66]. The recent trend has been increasing catalyst activity with a lower cost and environmentally benign materials due to less energy demand for biomass reformation than photocatalytic water splitting.

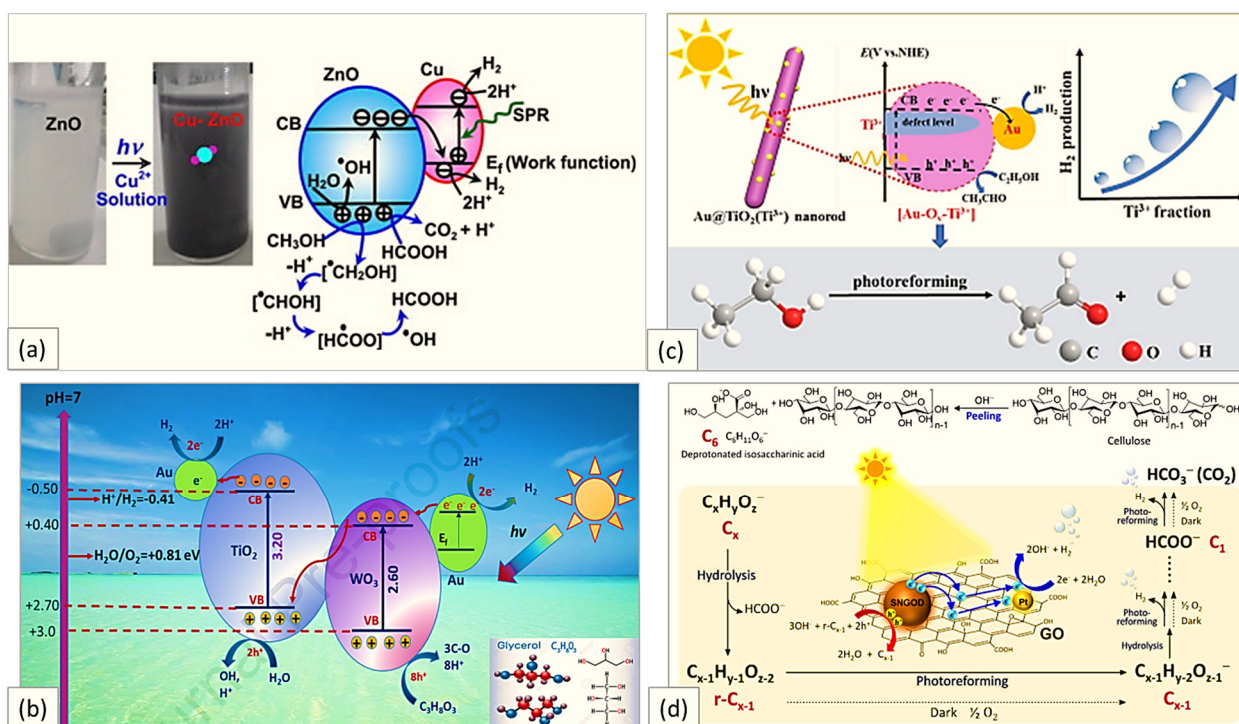


Figure 3. Illustration of mechanism involved in photoreforming of (a) methanol. Reprinted with permission from Elsevier Ref. [44] 2013, Paramasivan et al, (b) ethanol. Reprinted with permission from American chemical society Ref. [49], 2019, Xin Zhang et al, (c) glycerol. Reprinted with permission from Elsevier Ref. [54], 2020, Muhammad et al and (d) cellulose. Reprinted with permission from American chemical society Ref. [58], 2021, Van-Can et al.

4. Importance of Carboxylic Acids

As discussed in the previous section, along with alcohols, biomass, polysaccharides and carboxylic acids have been used as promising sacrificial agents in the photoproduction of H₂. Alcoholic photoreforming proceeds through the abstraction of a hydrogen atom by a OH[•] radical from the methylene group and aldehydes. Therefore, alcoholic organic molecules decompose through the formation of carboxylic acid [67]. Furthermore, researchers have proved that carboxylic acid photoreforming into H₂ production starts with a hole transfer to the carboxylic group instead of H abstraction from OH[•]. The carboxylic functionality is one of the oxygen-containing groups with excellent absorption and better reactivity in the photoreforming process [68]. Therefore, today, carboxylic acids are used as sacrificial agents for H₂ production with hydrocarbons. Carboxylic acids are the intermediates in various reactions, such as hemicellulose derived from biomass, and the hydrolysis/pyrolysis of lignocellulose produces carboxylic acids, i.e., formic acid (FA) and acetic acid [69]. Moreover, the fermentation of saccharides produces carboxy functionality (lactic acid). In the photoreforming of acids, researchers have used direct or indirect acids (direct acids as a source and indirect acids as intermediates produced from biomass). In this process, the reaction occurs by binding the carboxylates to the photocatalyst surface, which processes decarboxylation, resulting in the formation of carbon dioxide followed by proton reduction into H₂.

The CO₂ evolution occurs via photo-Kolbe-type decarboxylation through carboxyl radicals. The efficiency of this process mainly depends on the design of the photocatalyst, reaction system, irradiation time and pH of the solution [70]. Various photocatalysts have been used for the degradation of carboxylic acids; most commonly, TiO₂ has been introduced effectively in photoreforming due to its cost-effective, chemical and photochemical stabilities. TiO₂ has been modified with various noble metals to obtain a significant hydrogen evolution rate. Yuexiang Li et al. investigated the evolution of hydrogen using oxalic acid on a Pt-decorated TiO₂ catalyst, and the efficiency of Pt/TiO₂ was carried out using oxalic acid, formic acid and formaldehyde [71,72]. Furthermore, the modification of TiO₂ was performed using alkaline earth metals such as calcium, strontium and barium to enhance photocatalytic hydrogen evolution using formic acid, acetic acid and formaldehyde [73]. Various metal sulfides and oxides such as cadmium sulfides, vanadium pentoxides, iron oxides, zinc oxides and zinc sulfides are reviewed systematically in further individual sections on acid photoreforming.

4.1. Formic Acid

Formic acid (FA) is colorless, less toxic and completely biodegradable [74], and it can be stored/used at room temperature. Therefore, FA is the easiest root for hydrogen generation, with a higher volumetric and gravimetric H₂ evolution capacity. This acid can be produced from photo-electrocatalytic CO₂ reduction and the decomposition of biomass [75]. H₂ generation during FA photoreforming and selectivity is an important aspect on which H₂ evolution quality depends, along with reaction conditions, catalyst materials and temperature. Since the early 20th century, various studies using FA have developed several homogeneous and heterogeneous photocatalysts. TiO₂ semiconducting materials have been used for H₂ production by modifying them using noble metals as co-catalysts to enhance the efficiency of the photocatalysts. The combination of semiconductors with noble metals has been studied for photocatalytic FA degradation in H₂ production with a higher quantum yield and a high production rate. Yuexiang Li et al. used Pt/TiO₂ for H₂ production through FA photoreforming. The overall H₂ evolution rate was consistent with that of the decomposition of FA [72]. Chen Tao et al. used Pt/TiO₂ for the anaerobic photocatalytic degradation of FA. In this reaction, adsorbed molecules of FA converted into formate species and transformed into carbonate species with the further formation of H₂ while adding water vapor into the reaction media [76]. Alexia Patsoura et al. used Pt/TiO₂ as a photocatalyst for the photoreforming of alcohol and organic acid [17]. Furthermore, Chiarello et al. investigated the formation of H₂ using noble metals Au-, Ag- and Au-

Ag-modified TiO₂ with methanol steam with the formation of FA as an intermediate for H₂ production. There are various byproducts that are formed, such as carbon monoxide, methane, acetaldehyde and methyl formate, with constant rates of H₂ evolution and CO₂ formation [39]. Furthermore, Valeriano Lanese et al. developed copper-doped TiO₂ for aqueous FA photoreforming. The oxidation states of Cu affect the efficiency of hydrogen production. Zerovalent Cu does not affect hydrogen evolution, and cupric ions enhance the rate and quantity of hydrogen production while maintaining the experimental parameters in both the reactions [77]. Hainer et al. reported various metal-doped (Cu, Ru, Pt and Au) TiO₂ for hydrogen evolution using methanol and FA. In this study, Pt/TiO₂ showed higher H₂ production using methanol. Cu/TiO₂ and Ru/TiO₂ showed higher yields towards hydrogen production using FA. Au/TiO₂ was responsible for the high rate of hydrogen production using FA [78].

Jamal et al. selectively produced hydrogen photo-catalytically from FA efficiently using non-noble metals, such as cobalt and nickel, as redox mediators on CdS nanorods, as shown in the following. The effect of co-catalysts was also studied on the decomposition of FA. Here, the high hydrogen production of 32.6 mmol h⁻¹g⁻¹ from FA was obtained by sustaining the production rate for 12 h [79]. The mechanism involved a substantial increase in FA-to-H₂ activity for Ni/CdS-NR, the quenching of the PL signal and the reduction of Ni²⁺ to Ni⁰ in the reaction system by photogenerated electrons at the CB of CdS. This band offset between CdS and Ni⁰ provides a conduit for electrons to pass from CdS to Ni⁰. The Co is not deposited on the CdS, but it is present in the reaction media. The observed enhanced activity presumably occurs through transitory contact with the CdS, forming a bound Co-hole formate species. Therefore, the improved catalysis is due to the cooperative redox mediation of Ni⁰ and Co³⁺, where both the reductive and oxidative half-reactions are enhanced, as shown in Figure 4. Further various co-catalysts are developed to increase hydrogen production with great sustainability, which are discussed in Table 1.

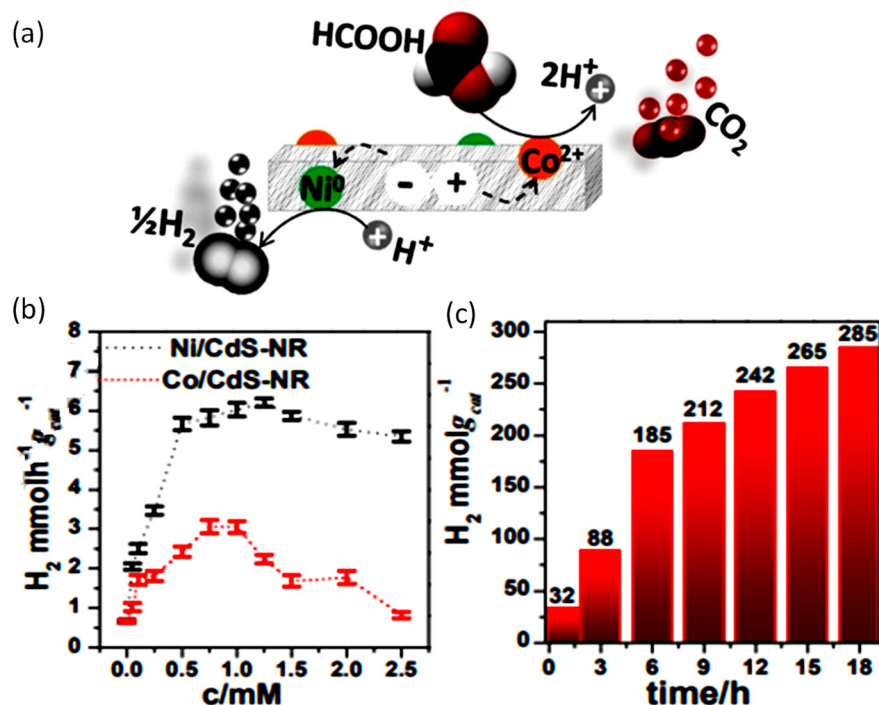


Figure 4. (a) Photoreforming of FA on NiCo/CdS; (b) Effect of Ni and Co on the production of H₂; (c) Long-term H₂ production using NiCo/CdS. Reprinted with permission from Elsevier Ref. [79], 2018, M. Abdullah Khan et al.

Table 1. Illustration of various catalysts, light sources and cocatalysts used in the photoreforming of FA (HCOOH) and the rate of hydrogen production.

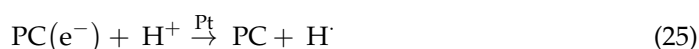
Concentration	Light Source, Wavelength (nm)	Photocatalyst	Co-Catalyst	Time Course (h)	Rate of Production ($\mu\text{molg}^{-1} \text{h}^{-1}$)			Reference
					H ₂	CO ₂	CO	
<i>aq.</i> 1.3 mM	solar	0.5%-Pt/TiO ₂	Pt	20	1275	-	-	[17]
<i>aq.</i> 0.01 M	Hg	0.5%-Pt/TiO ₂	Pt	5	1150	-	-	[72]
H ₂ O/HCOOH (10:1), <i>v</i>	Hg, 350–450	FP-0.5%-Pt/TiO ₂	Pt	-	5400	4100	80	[80]
10 vol%, (35 °C)	UV light, 200–800	1%-Pt/TiO ₂	Pt (photo)	8	61.5	-	-	[81]
10 vol%, (90 °C)	UV light	1%-Pt/TiO ₂	Pt (thermal)	8	119.3	-	-	[81]
10 vol%, (photo + 90 °C)	UV light	1%-Pt/TiO ₂	Pt (photo-thermal)	8	499.8	-	-	[81]
0.5 M HCO ₂ ⁻ /H ₂ O	UV light	CdS	-	12	420 (μL)	-	-	[82]
0.5 M DCO ₂ ⁻ /H ₂ O	UV light	CdS	-	12	110 (μL)	-	-	[82]
<i>aq.</i> , 5 mL of 88% HCOOH	Hg, >300	1.5%-Pt/CdS (photoetching)	Pt	10	1128	-	-	[83]
<i>aq.</i> , 5 mL of 88 wt% HCOOH	Hg	CdS	-	10	79	-	-	[83]
<i>aq.</i> , 5 mL of 88 wt% HCOOH	Hg, 420	0.05%-Pt/CdS	Pt	10	4460	-	-	[84]
<i>aq.</i> , 5 mL of 88 wt% HCOOH	Hg	CdS	-	10	219	-	-	[84]
<i>aq.</i> , 2 M	Hg, 400	Pt/CdS	Pt	20	385	385	77	[85]
<i>aq.</i> , 20 mL	Xe, >420	Co-Ni/CdS-NR	Co, Ni	18	32,600	-	-	[79]
<i>aq.</i> , 20 mL	Xe	Co/CdS-NR	Co	12	14,200	-	-	[79]
<i>aq.</i> , 20 mL	Xe	Ni/CdS-NR	Ni	12	22,800	-	-	[79]
<i>aq.</i> , 20 mL	Xe	CdS-NR	-	12	13,400	-	-	[79]
<i>aq.</i> , 2.7 M	Solar, 420–780	0.75%-Au, 0.25%-Pd/TiO ₂	Au, Pd	10	17,700	-	-	[86]
<i>aq.</i> , 200 mL of 2.5 vol% CHOOH	Hg	1%-Au-loaded mesoporous assembled SrTiO ₃	Au	5	647	-	-	[87]
<i>aq.</i> , 150 mL H ₂ O + HCOOH	Xe	CdS-ZnS	Cd:Zn (0.8:0.2)	4	1263	-	-	[88]
<i>aq.</i> , 150 mL H ₂ O + HCOOH	Xe	5%-Ru/CdS-ZnS	Ru, Cd:Zn (0.8:0.2)	4	5800	-	-	[88]
<i>aq.</i> , 200 mL, 0.05 M	Xe, <355	Au/TiO ₂	Au	4	452	-	-	[89]
<i>aq.</i> , (4:1 in volume) H ₂ O:HCOOH	Xe, <420	0.34%-Pt/2.5%-CdS/Al-HMS	Pt	6	1705	-	-	[90]

Table 1. Cont.

Concentration	Light Source, Wavelength (nm)	Photocatalyst	Co-Catalyst	Time Course (h)	Rate of Production ($\mu\text{molg}^{-1} \text{h}^{-1}$)			Reference
					H ₂	CO ₂	CO	
aq, (9:1 in volume) H ₂ O:HCOOH	Xe, <420	0.99%Ru/21%-CdS/Al-HMS	Ru	6	2753	-	-	[91]
aq, 1 M	Hg, 399	SrTiO ₃ :TiO ₂	SrTiO ₃	5	280	-	-	[73]
aq, 2.5 M	UV light, >420	QD-MPA	-	168	52,100	-	-	[92]
aq, 2.5 M	UV light	QD-MPA/CoCl ₂	CoCl ₂	168	116,000	-	-	[92]
aq, 20 vol% HCOOH	UV light	0.01%-Pt/CdS/TNT	Pt	3	42,600	-	-	[93]
aq, 10 vol% HCOOH	UV light, 254	1%-Pt(P)/CdS/TNT	Pt	3	3300	-	-	[94]
5 mL HCOOH in 100 mL H ₂ O + 180 °C	UV light, \geq 420	0.025%-Pt/CdS-QD	Pt	30	12,200	-	-	[95]
aq, 10 mL, 1 M HCOOH	UV light, \geq 420	Pd/C ₃ N ₄	Pd	6	53,400	-	-	[96]
aq, 1 M HCOOH	UV light	Cu/TiO ₂ (anatase)	Cu	5	5000	-	-	[77]
aq, 2.5 M HCOOH, pH 5	Halogen, 420	0.5%-Pt/Cu ₂ O	Pt	40	155	158	-	[97]
aq, 2.5 M HCOOH, pH 5	Halogen	Cu ₂ O	-	40	65	64	-	[97]
1 mL DMF, 5 mL 5HCO ₂ H · 2NEt ₃	Xe	[Fe ₃ (CO) ₁₂] + PPh ₃ , 2,2':6',2''-terpyridine		3	2700	-	trace	[98]

4.2. Acetic Acid

Most of the studies have employed organic acids as electron donors in hydrogen production in the photoreforming process as acetic acid, since it is a common organic molecule in industrial waste [99]. The use of acetic acid to produce H₂ allows the environment-friendly pathway by wastewater treatment with desired valuable products. The degradation of acetic acid through the photoreforming process into valuable products is revolutionary, as it does not require a high capital cost. The use of acetic acid as a sacrificial agent in photocatalysis leads to the formation of H₂ and various hydrocarbons, such as CH₄ and C₂H₆, which can be further used as renewable fuels [100]. Various studies have been reported by Krauetler and Bard, which discuss the photocatalytic conversion of acetic acid into H₂ and byproducts as hydrocarbons over Pt/TiO₂ in acidic conditions. Initially, the decomposition of acetic acid using visible light results in the production of CH₄ and CO₂ due to a more favorable thermodynamic nature, as compared to the reforming of acetic acid [101]. The following scheme shows a plausible reaction pathway for aqueous acetic acid photocatalytic transformation on the photocatalyst surface.





Formation of $\cdot\text{CH}_3$ and $\cdot\text{C}_2\text{H}_5$



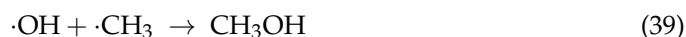
Formation of molecular hydrogen and alkanes (Kolbe products)



Formation of $\text{C}_2\text{H}_5\text{COOH}$



Formation of alcohols (Hofer–Moest products)



In these studies, the amount of hydrogen production is seen to be lower, therefore increasing the efficiency of the reaction towards the high quantity production of H_2 . Hlroshl et al. demonstrated the photoreforming of acetic acid into valuable products (i.e., CH_4 H_2) using Pt/ TiO_2 suspensions at various pH. The main reaction product observed was methane but increased the H_2/CH_4 ratio by increasing the pH [102]. Tadayoshi Sakata et al. studied the heterogeneous photocatalyst for the reaction of acetic, propionic and butyric acid on different semiconducting materials. The type of semiconductor and pH of the reaction system was studied. The production of hydrocarbons had completely stopped, and H_2 evolution was increased by increasing the pH from acidic to neutral and alkaline. This study predicted that the position of the valence band of the semiconducting material depends on the pH and that the reaction path is controlled by the amount of OH^\cdot ions [100]. Xian-Jun Zheng et al. reported the photocatalysis of acetic acid over Pt/ TiO_2 in UV radiation. The effects of various parameters were checked with an optimal amount of photo-deposited Pt on TiO_2 [103]. In addition, CuO/SnO_2 as the photocatalyst for acetic acid reformation into H_2 has been used [104]. Recently, Mikel Imizcoz et al. reported an earth-abundant co-catalyst on TiO_2 for the selective production of H_2 from acetic acid derived from biomass feedstocks. They reported higher decarboxylation activity due to copper nanoparticle insertion in semiconducting materials and also that the selectivity of H_2 production increases with photo-deposited Cu in aqueous acetic suspensions as compared to Pt/ TiO_2 [105]. The simple mechanisms are depicted in Figure 5. Upon solar irradiation, photogenerated electrons from the CB of TiO_2 are capable of moving to CuO nanoparticles and reducing them. H_2 evolution increased marginally as copper mass loading increased due to the maximized surface reduction of copper. Various co-catalysts with semiconducting materials for acetic acid reforming are listed below in Table 2.

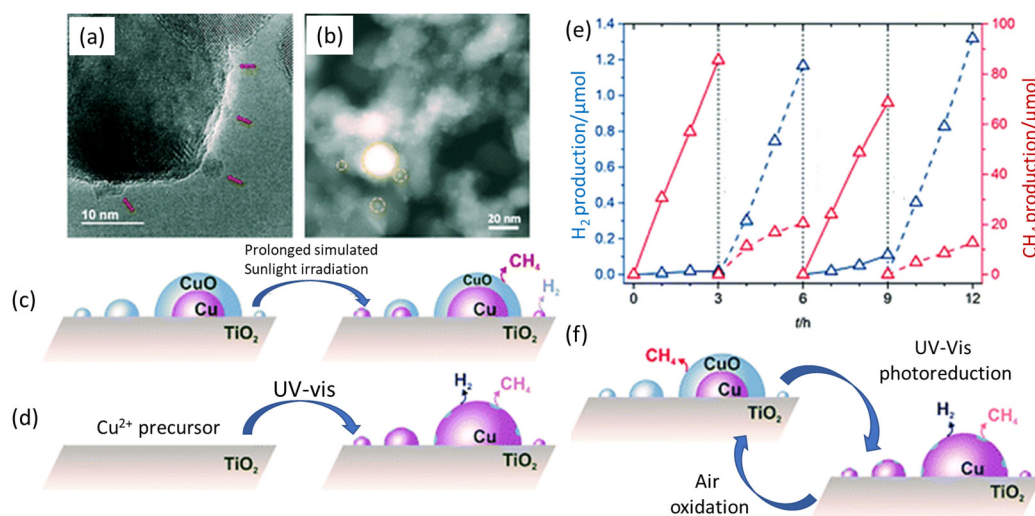


Figure 5. (a,b) TEM images of copper-loaded TiO₂; (c,d) Mechanism involved in the production of hydrogen using acetic acid as a sacrificial agent; (e) H₂ and CH₄ production for 12 h on Cu/TiO₂; (f) Overall mechanism that occurs in the photoreforming of acetic acid on Cu/TiO₂ [105].

Table 2. Illustration of various catalysts, light sources and cocatalysts used in the photoreforming of acetic acid (CH₃COOH) and the rate of hydrogen production.

Concentration	Light Source, Wavelength (nm)	Photocatalyst	Co-Catalyst	Time Course (h)	Rate of Production (μmol g ⁻¹ h ⁻¹)				Reference
					H ₂	CO ₂	CH ₄	C ₂ H ₆	
aq, 1 M CH ₃ COOH	UV light	Ln ³⁺ (0.02%-Eu)/TiO ₂	Ln ³⁺ (Eu ³⁺)	27	9	88	108	4	[106]
aq, 1 M CH ₃ COOH	UV light	Ln ³⁺ (0.05%-Sm)/TiO ₂	Ln ³⁺ (Sm ³⁺)	27	3	131	124	3	[106]
aq, 0.87 mM CH ₃ COOH	Xe	0.5%-Pt/P25TiO ₂	Pt	20	278	-	-	-	[17]
aq, H ₂ O/CH ₃ COOH (5:1)	Hg	0.5%Pt/PEG-TiO ₂	Pt	6	1000	-	-	-	[107]
aq, H ₂ O/CH ₃ COOH (10:1)	Hg	0.6%-Pt/TiO ₂ (mesoporous)	Pt	5	390	-	-	-	[108]
aq, 50 mL (0.5 M) CH ₃ COOH and H ₂ O, pH 2	Xe	1%-Pt/TiO ₂	Pt	15	22 (μmol/h)	65 (μmol/h)	35 (μmol/h)	2 (μmol/h)	[109]
aq, 450 mL CH ₃ COOH (4.35 g/L), pH 1.0	Hg	1%Pt-TiO ₂	Pt	4	28,478	-	-	-	[103]
l, 15 mL solution CH ₃ COOH/Na HAC	Xe-Hg	1-5%-Pt/TiO ₂ (anatase)	Pt		-	1600	-	-	[101]
l, H ₂ O/CH ₃ COOH (1:9)	Xe-Hg	1-5%-Pt/TiO ₂ (anatase)	Pt		-	4060	-	-	[101]
l, H ₂ O/CH ₃ COOH (1:1)	Xe-Hg	1-5%-Pt/TiO ₂ (anatase)	Pt		-	1563	1322	120	[101]

Table 2. Cont.

Concentration	Light Source, Wavelength (nm)	Photocatalyst	Co-Catalyst	Time Course (h)	Rate of Production ($\mu\text{molg}^{-1} \text{h}^{-1}$)				Reference
					H ₂	CO ₂	CH ₄	C ₂ H ₆	
<i>aq</i> , AcOH/Na [AcO] (4:0.6 M), pH 3.9	Hg-conc.	3%-Pt/TiO ₂ (anatase)	Pt		24	65	43	4	[102]
<i>aq</i> , AcOH/Na [AcO] (4:0.6 M), pH 3.9	Hg-conc.	3%-Pt/TiO ₂ (rutile)	Pt		9	11	10	1	[102]
<i>v</i> , CH ₃ COOH (11 torr)	Hg	2%- Pt/TiO ₂ (anatase)	Pt	3	46	132	54	43	[110]
<i>v</i> , H ₂ O/CH ₃ COOH (24:11 torr)	Hg	2%- Pt/TiO ₂ (anatase)	Pt	3	180	453	104	180	[110]
<i>l</i> , CH ₃ COOH (1 mL)	Hg	2%- Pt/TiO ₂ (anatase)	Pt	3	46	290	163	12	[110]
<i>l</i> , H ₂ O/CH ₃ COOH (6:1), pH 2.1	Hg, 366	7%-Pt/TiO ₂ (rutile)	Pt		77	-	397	-	[111]
<i>l</i> , H ₂ O/CH ₃ COOH (6:1), pH 8.8	Hg	7%-Pt/TiO ₂ (rutile)	Pt		367	-	2	-	[111]
<i>aq</i> , Na (AcO) (1.7% <i>w/v</i>), pH 7.4	Hg	7%-Pt/TiO ₂ (anatase)	Pt		165	27	0.24	-	[111]
<i>aq</i> , 1 M CH ₃ COOH, pH 2.6	UV light	10%- Cu/TiO ₂	Cu	5	144	640	590	66	[112]
<i>aq</i> , 1 M CH ₃ COOH	UV light, 366	P ²⁵ TiO ₂		27	2	141	50	4	[113]
<i>aq</i> , 1 M CH ₃ COOH	UV light, 366	10%-Fe/TiO ₂	Fe	27	7	102	93	4	[113]
<i>aq</i> , 1 M CH ₃ COOH	Hg	20%-Fe/TiO ₂	Fe	5	7	257	260	15	[114]
<i>v</i> , CH ₃ COOH (665 Pa)	Hg-Xe, >420	TiO ₂	-		-	0.370	0.018	-	[115]
<i>v</i> , CH ₃ COOH (665 Pa)	Hg-Xe	ZnO ₂	-		-	0.098	0.034	-	[115]
<i>v</i> , CH ₃ COOH (665 Pa)	Hg-Xe	MgO	-		-	0.923	0.179	-	[115]
<i>v</i> , CH ₃ COOH (665 Pa)	Hg-Xe	SiO ₂	-		-	0.336	0.168	-	[115]
<i>v</i> , CH ₃ COOH (665 Pa)	Hg-Xe	WO ₃	-		-	0.026	0.03	-	[115]
<i>v</i> , CH ₃ COOH (665 Pa)	Hg-Xe	γ -Al ₂ O ₃	-		-	0.336	0.086	-	[115]

4.3. Lactic Acid

Lactic acid (LA) is an industrial product, and the polymers derived from acetic acid are biodegradable and can be synthesized from the fermentation of carbohydrates and biomass. LA has been used in several medical, textile and pharmaceutical industries [116]. LA is employed as a supplement in the synthesis of pharmaceuticals as well as in the production of hygiene and cosmetic goods in the cosmetics sector [117]. Due to this industrial application, LA is absorbed into water bodies. The purification of water, as well

as the removal of LA, is needed. To overcome these issues, there must be reformation of LA into valuable products and hydrogen fuel. There are various strategies to produce H₂, such as photon-assisted water splitting and the photoreforming process. LA is used as a sacrificial agent in the photo-production of H₂ [118]. As discussed in the previous section, co-catalyst-assisted semiconducting materials are used as photocatalysts in the photoreforming process. Initially, Harada et al. found the decomposition of LA over platinized CdS and TiO₂. The obtained quantum efficiencies for the Pt/TiO₂ and Pt/CdS were 71% (360 nm) and 38% (440 nm). The products obtained during the photocatalytic decomposition of LA on Pt/TiO₂ were acetaldehyde, carbon dioxide and hydrogen, and by using Pt/CdS, they were hydrogen and pyruvic acid [119,120].

Furthermore, LA photoreforming was carried out using a non-noble cost-effective metal as a cocatalyst with cadmium sulfides as the photocatalysts under visible light. Wei Zhang et al. reported the quantum efficiency for H₂ production of 51.3% under the visible light range (420 nm) [120]. Qin et al. investigated photoreforming using LA as a sacrificial agent on a CdS cluster-decorated graphene nanosheet as a photocatalyst and Pt as a co-catalyst. The photoreforming was carried out under visible radiation with an increase in the rate and quantity of H₂ by increasing the content of graphene in the catalyst compared to bare CdS due to an increase in crystallinity and surface area. They reported that the use of CdS as a photo-corrosive agent and of a Pt co-catalyst reduces overpotential in H₂ production and opposes the backward combination reactions with a high rate of H₂ (1.12 m mol h⁻¹) and 22.5% of quantum efficiency at 420 nm [121]. Xu Zong et al. demonstrated that MoS₂-loaded CdS catalyst showed a higher rate and quantity of H₂ evolution from LA under visible light. MoS₂/CdS was increased 36 times more than the bare CdS and had higher activity than the Pt/CdS [122]. Zhuofeng Hu et al. produced an innovative photocatalyst as a platinum cobalt alloy on CdS and TiO₂ by a simple polyol reduction method. The introduction of cobalt as a cocatalyst with Pt increased composite conductivity, resulting in enhanced H₂ evolution from acetic acid decomposition on Pt₃Co/CdS and Pt₃Co/TiO₂ under visible light radiation with 15.86 and 13.01 m mol g⁻¹ h⁻¹, respectively [123]. Recently, Chunhe Li loaded NiS nanoparticles on CdS through solvothermal synthesis and used as a catalyst for the evolution of hydrogen from lignin and LA as a hole scavenger. The activity of NiS/CdS is 5041 time more than the bare CdS and has an apparent quantum efficiency of 44.9% for hydrogen evolution with five repetitive cycles [124]. This report, as shown in Figure 6c, generated charge carriers in CdS when it was excited with light. Even though the CB band of CdS is more negative than the reduction potential of H⁺/H₂, the rate of hydrogen evolution is low on CdS because of the fast recombination of photoinduced charge carriers. When the NiS nanoparticles are loaded on the surface of CdS, because of the less negative CB of NiS than that of CdS, photogenerated charge carriers transfer to the NiS nanoparticles. Mainly, the intimate interfacial junction between NiS and CdS plays an essential role in facilitating the transmitting of electrons from CdS to NiS. NiS acts as an active site because the unsaturated sulfide ions of NiS possess more affinity towards H⁺ and thus enhance hydrogen evolution. The details of the photoreforming of LA in the coexistence of lignin under visible light radiation are described in Figure 6. Various reports on photoreformation of LA are tabulated in Table 3.

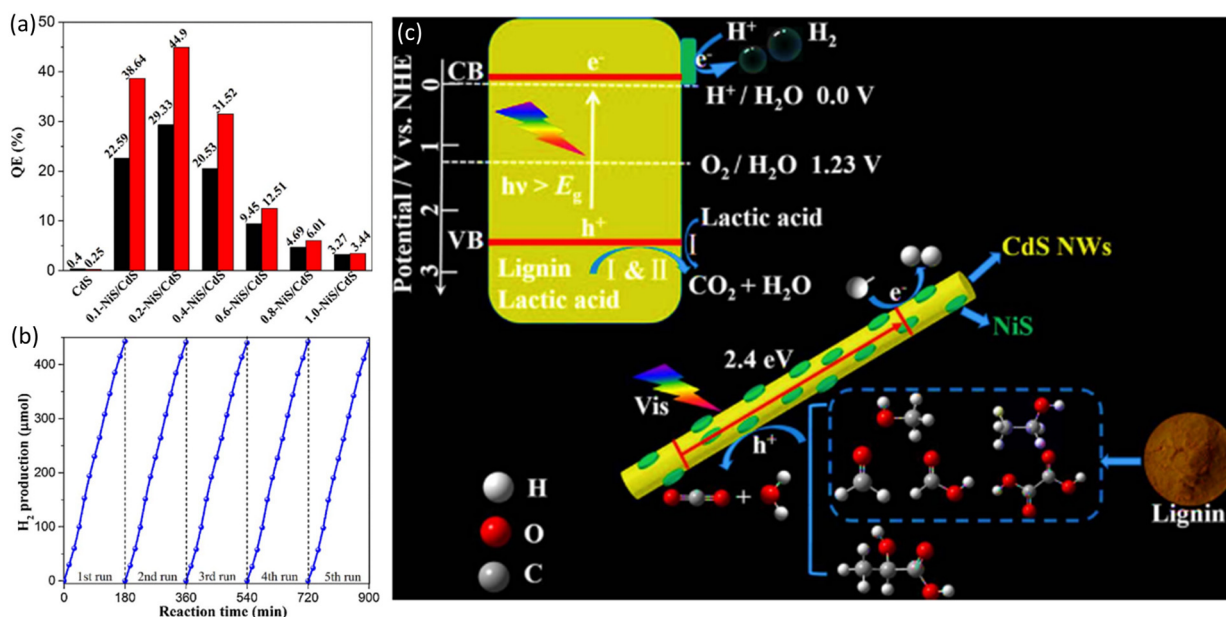


Figure 6. (a) Comparison of the quantum efficiency of hydrogen production on NiS/CdS using lignin and LA as a sacrificial agent; (b) Long-term stability of the production of H₂ on a NiS/CdS photocatalyst; (c) Mechanism involved in the lignin and LA reformation of NiS/CdS photocatalysts. Reprinted with permission from Elsevier Ref. [124], 2018, Chunhe Li et al.

Table 3. Illustration of various catalysts, light sources and co-catalysts used in photoreforming of LA (CH₃CH(OH)COOH) and the rate of hydrogen production.

Concentration	Light Source, Wavelength (nm)	Photocatalyst	Co-Catalyst	Time Course (h)	Rate of Production (μmol g ⁻¹ h ⁻¹)		Reference
					H ₂	CO ₂	
CH ₃ CH(OH)COOH/H ₂ O (1:10) pH 2	<i>I_v</i> , Xe, 360–520	5%-Pt/TiO ₂ (rutile)	Pt	4	1008	1192	[120]
CH ₃ CH(OH)COOH/H ₂ O (1:10) pH 2	<i>I_v</i> , Xe	5%-Pt/CdS	Pt	4	1000	13	[120]
CH ₃ CH(OH)COOH/H ₂ O (1:9)	<i>I_v</i> , Xe, 420	1%-Pt/CdS	Pt		8170	-	[123]
CH ₃ CH(OH)COOH/H ₂ O (1:9)	<i>I_v</i> , Xe	1%-(Pt ₃ Co)/CdS	Pt, Co		15,860	-	[123]
CH ₃ CH(OH)COOH/H ₂ O (1:9)	<i>I_v</i> , Xe	1%-(Pt _{2.3} -Co)/CdS	Pt, Co		13,010	-	[123]
CH ₃ CH(OH)COOH/H ₂ O (1:9)	<i>I_v</i> , Xe	1%-(PtCo)/CdS	Pt, Co		7050	-	[123]
CH ₃ CH(OH)COOH/H ₂ O (1:9)	<i>I_v</i> , Xe	1%-Co/CdS	Co		1070	-	[123]
CH ₃ CH(OH)COOH/H ₂ O (1:9)	<i>I_v</i> , Xe	1%-(Pt ₃ Au)/CdS	Pt, Au		14,900	-	[123]
CH ₃ CH(OH)COOH/H ₂ O (1:9)	<i>I_v</i> , Xe	1%-(Pt ₃ Ni)/CdS	Pt, Ni		12,810	-	[123]

Table 3. Cont.

Concentration	Light Source, Wavelength (nm)	Photocatalyst	Co-Catalyst	Time Course (h)	Rate of Production ($\mu\text{mol g}^{-1} \text{h}^{-1}$)		Reference
					H ₂	CO ₂	
$\text{CH}_3\text{CH}(\text{OH})\text{COOH}/\text{H}_2\text{O}$ (1:9) <i>l</i> ,	Xe	1%-(Pt ₃ Cu)/CdS	Pt, Cu		3890	-	[123]
$\text{CH}_3\text{CH}(\text{OH})\text{COOH}/\text{H}_2\text{O}$ (1:9) <i>l</i> ,	Xe	1%-Pt/ ^{P25} TiO ₂	Pt		690	-	[123]
$\text{CH}_3\text{CH}(\text{OH})\text{COOH}/\text{H}_2\text{O}$ (1:9) <i>l</i> ,	Xe	1%-(Pt ₃ Co)/ ^{P25} TiO ₂	Pt, Co		1040	-	[123]
$\text{CH}_3\text{CH}(\text{OH})\text{COOH}/\text{H}_2\text{O}$ (1:9) <i>l</i> ,	Xe	1%-(Pt ₃ Au)/ ^{P25} TiO ₂	Pt, Au		890	-	[123]
$\text{CH}_3\text{CH}(\text{OH})\text{COOH}/\text{H}_2\text{O}$ (1:9) <i>l</i> ,	Xe	1%-(Pt ₃ Ni)/ ^{P25} TiO ₂	Pt, Ni		820	-	[123]
$\text{CH}_3\text{CH}(\text{OH})\text{COOH}/\text{H}_2\text{O}$ (1:9) <i>l</i> ,	Xe, 420	1%-(Pt ₃ Cu)/ ^{P25} TiO ₂	Pt, Cu		460	-	[123]
$\text{CH}_3\text{CH}(\text{OH})\text{COOH}/\text{H}_2\text{O}$ (1:9) <i>l</i> ,	Xe	0.2%-MoS ₂ /CdS	MoS ₂		5400	-	[125]
$\text{CH}_3\text{CH}(\text{OH})\text{COOH}/\text{H}_2\text{O}$ (1:9) <i>l</i> ,	Xe	0.2%-Pt/CdS	Pt	5	4400	-	[125]
$\text{CH}_3\text{CH}(\text{OH})\text{COOH}/\text{H}_2\text{O}$ (1:9) <i>l</i> ,	Xe	0.2%-Ru/CdS	Ru	5	3650	-	[125]
$\text{CH}_3\text{CH}(\text{OH})\text{COOH}/\text{H}_2\text{O}$ (1:9) <i>l</i> ,	Xe	0.2%-Rh/CdS	Rh	5	2500	-	[125]
$\text{CH}_3\text{CH}(\text{OH})\text{COOH}/\text{H}_2\text{O}$ (1:9) <i>l</i> ,	Xe	0.2%-Pd/CdS	Pd	5	1800	-	[125]
$\text{CH}_3\text{CH}(\text{OH})\text{COOH}/\text{H}_2\text{O}$ (1:9) <i>l</i> ,	Xe	0.2%-Au/CdS	Au	5	400	-	[125]
$\text{CH}_3\text{CH}(\text{OH})\text{COOH}/\text{H}_2\text{O}$ (1:9) <i>l</i> ,	Xe, 420	CdS	-	5	150	-	[125]
$\text{CH}_3\text{CH}(\text{OH})\text{COOH}/\text{H}_2\text{O}$ (1:9) <i>l</i> ,	Xe, 420	1%-WS ₂ /CdS	WS ₂	5	4000	-	[122]
$\text{CH}_3\text{CH}(\text{OH})\text{COOH}/\text{H}_2\text{O}$ (1:9) <i>l</i> ,	Xe	1%-Pt/CdS	Pt	5	3550	-	[122]
$\text{CH}_3\text{CH}(\text{OH})\text{COOH}/\text{H}_2\text{O}$ (1:9) <i>l</i> ,	Xe	1%-Ru/CdS	Ru	5	2930	-	[122]
$\text{CH}_3\text{CH}(\text{OH})\text{COOH}/\text{H}_2\text{O}$ (1:9) <i>l</i> ,	Xe	1%-Rh/CdS	Rh	5	2070	-	[122]
$\text{CH}_3\text{CH}(\text{OH})\text{COOH}/\text{H}_2\text{O}$ (1:9) <i>l</i> ,	Xe	1%-Au/CdS	Au	5	455	-	[122]

Table 3. Cont.

Concentration	Light Source, Wavelength (nm)	Photocatalyst	Co-Catalyst	Time Course (h)	Rate of Production ($\mu\text{mol g}^{-1} \text{h}^{-1}$)		Reference
					H ₂	CO ₂	
H ₂ O/CH ₃ CH(OH)COOH (10:1) <i>aq</i> ,	Xe	0.9%-MoS ₂ /CdS	MoS ₂	5	13,151	-	[126]
H ₂ O/CH ₃ CH(OH)COOH (10:1) <i>aq</i> ,	Xe, 420	0.2%-Pt/CdS	Pt	5	4880	-	[126]
H ₂ O/CH ₃ CH(OH)COOH (9:1) <i>aq</i> ,	Xe, 420	2.5%-MoS ₂ - RGO/CdS	MoS ₂ -RGO		621.3	-	[127]
H ₂ O/CH ₃ CH(OH)COOH (9:1) <i>aq</i> ,	Xe	2.5%-MoS ₂ /CdS	MoS ₂		551.3	-	[127]
H ₂ O/CH ₃ CH(OH)COOH (9:1) <i>aq</i> ,	Xe	0.25%-Pt/CdS	Pt		450	-	[127]
H ₂ O/CH ₃ CH(OH)COOH (9:1) <i>aq</i> ,	Xe, 420	1.5%- RGO/CdS/1.5%- MoS ₂	RGO, MoS ₂	5	1980	-	[128]
H ₂ O/CH ₃ CH(OH)COOH (4:1) <i>aq</i> ,	Xe, 420	2%- (MoS ₂ /RGO)/CdS	MoS ₂ , RGO	5	9000	-	[129]
H ₂ O/CH ₃ CH(OH)COOH (7:3) <i>aq</i> ,	Xe, 420	1.2%-NiS/CdS	NiS		7267	-	[118]
H ₂ O/CH ₃ CH(OH)COOH (7:3) <i>aq</i> ,	Xe, 420	CdS	-		210	-	[118]
H ₂ O/CH ₃ CH(OH)COOH (7:3) <i>aq</i> ,	Xe	1%-Pt/CdS	Pt		1333	-	[118]
H ₂ O/CH ₃ CH(OH)COOH (7:3) <i>aq</i> ,	Xe	1.2%-CoS/CdS	CoS		1000	-	[118]
H ₂ O/CH ₃ CH(OH)COOH (9:1) <i>aq</i> ,	Xe, 420	TiO ₂ -1.2%- Pt/CdS	Pt, TiO ₂ NPs		14,750	-	[130]
H ₂ O/CH ₃ CH(OH)COOH (9:1) <i>aq</i> ,	Xe	P ²⁵ TiO ₂ - 2%Pt/Cds	Pt, TiO ₂ NPs		13,750	-	[130]
H ₂ O/CH ₃ CH(OH)COOH (9:1) <i>aq</i> ,	Xe, 420	2%-Pt/P ²⁵ TiO ₂			3875	-	[130]
H ₂ O/CH ₃ CH(OH)COOH (9:1) <i>aq</i> ,	Xe, 420	0.5%-Pt/0.5%- RGO/CdS	Pt, RGO		19,000	-	[121]
H ₂ O/CH ₃ CH(OH)COOH (9:1) <i>aq</i> ,	Xe	0.5%-Pt/1%- RGO/CdS	Pt, RGO		56,000	-	[121]
H ₂ O/CH ₃ CH(OH)COOH (9:1) <i>aq</i> ,	Xe	0.5%-Pt/2.5%- RGO/CdS	Pt, RGO		27,500	-	[121]
H ₂ O/CH ₃ CH(OH)COOH (9:1) <i>aq</i> ,	Xe, 420	0.2%-MoS ₂ /g- C ₃ N ₄ (mesoporous)	MoS ₂	4	1375	-	[131]

Table 3. Cont.

Concentration	Light Source, Wavelength (nm)	Photocatalyst	Co-Catalyst	Time Course (h)	Rate of Production ($\mu\text{mol g}^{-1} \text{h}^{-1}$)		Reference
					H ₂	CO ₂	
H ₂ O/CH ₃ CH(OH)COOH (9:1) <i>aq</i> ,	Xe	2%-Pt/g- C ₃ N ₄ (mesoporous)	Pt	4	1000	-	[131]
H ₂ O/CH ₃ CH(OH)COOH (9:1) <i>aq</i> ,	Xe	0.5%-WS ₂ /g- C ₃ N ₄ (mesoporous)	WS ₂	4	340	-	[131]
H ₂ O/CH ₃ CH(OH)COOH (9:1) <i>aq</i> ,	Xe, 420	Fe ₂ O ₃ -TiO ₂ -PtO _x	Fe ₂ O ₃ , PtO _x	5	1100	-	[132]
H ₂ O/CH ₃ CH(OH)COOH (7:3) <i>aq</i> ,	Xe, 280	5%- Pt/TaO _{2.18} Cl _{0.64}	Pt	8	1500	-	[133]
H ₂ O/CH ₃ CH(OH)COOH (19:1), pH 3 <i>aq</i> ,	LED, 420-780	CoP/CdS	CoP	10	251,500	-	[134]
H ₂ O/CH ₃ CH(OH)COOH (19:1), pH 3 <i>aq</i> ,	LED	Ni ₂ P/CdS	Ni ₂ P	10	143,600	-	[134]
H ₂ O/CH ₃ CH(OH)COOH (19:1), pH 3 <i>aq</i> ,	LED	Cu ₃ P/CdS	Cu ₃ P	10	77,600	-	[134]
H ₂ O/CH ₃ CH(OH)COOH (19:1), pH 3 <i>aq</i> ,	LED	Pt/CdS	Pt	10	77,300	-	[134]
H ₂ O/CH ₃ CH(OH)COOH (20:3) <i>aq</i> ,	LED, 420	Co _{0.85} Se/RGO- PEI nanosheets/CdS	Co _{0.85} Se/RGO- PEI nanosheets	10	17,600	-	[135]
H ₂ O/CH ₃ CH(OH)COOH (20:3) <i>aq</i> ,	LED	0.1%-Pt/CdS	Pt	10	18,600	-	[135]
H ₂ O/CH ₃ CH(OH)COOH (4:1) <i>aq</i> ,	Xe, 420	9%-CdS/1%- Pt/In ₂ O ₃	Pt	>10	9384	-	[136]
H ₂ O/CH ₃ CH(OH)COOH (4:1) <i>aq</i> ,	Xe	9%-CdS/1%- Pt/Ga ₂ O ₃	Pt	>10	9053	-	[136]
H ₂ O/CH ₃ CH(OH)COOH (4:1) <i>aq</i> ,	Xe, 420	9%-CdS/1%- Pt/P ₂₅ TiO ₂	Pt	>10	5482	-	[136]
H ₂ O/CH ₃ CH(OH)COOH (9:1) <i>aq</i> ,	Xe, 420	0.8%-NiB _x /CdS	NiB _x	10	4800	-	[137]
H ₂ O/CH ₃ CH(OH)COOH (9:1) <i>aq</i> ,	Xe, 420	9%-NiS-37%- CdS/Te	NiS, Te	12	317	-	[138]
H ₂ O/CH ₃ CH(OH)COOH (9:1) <i>aq</i> ,	Xe, 420	11%-Pt/11%- Pd/31%-CdS/Te	Pt, Pd, Te	12	236	-	[138]
H ₂ O/CH ₃ CH(OH)COOH (9:1) <i>aq</i> ,	Xe	1.5%-MoS ₂ /UiO- 66//CdS	MoS ₂	4	32,500	-	[139]
CH ₃ CH(OH)COOH (0.1 M) <i>aq</i> ,	Hg-Xe, 420	TiO ₂		3	0	693	[140]

Table 3. Cont.

Concentration	Light Source, Wavelength (nm)	Photocatalyst	Co-Catalyst	Time Course (h)	Rate of Production ($\mu\text{molg}^{-1} \text{h}^{-1}$)		Reference
					H ₂	CO ₂	
<i>aq</i> , CH ₃ CH(OH)COOH (0.1 M)	Hg-Xe	1%-Pt/TiO ₂	Pt	3	13,890	13,500	[140]
<i>aq</i> , CH ₃ CH(OH)COOH (0.1 M)	Hg-Xe	1%-Au/TiO ₂	Au	3	6667	6600	[140]
<i>aq</i> , CH ₃ CH(OH)COOH (0.1 M)	Hg-Xe	1%-Pd/TiO ₂	Pd	3	8300	8700	[140]
<i>aq</i> , CH ₃ CH(OH)COOH (0.1 M)	Hg-Xe	1%-Ru/TiO ₂	Ru	3	11,500	11,120	[140]

4.4. Other Carboxylic Acids

Including formic acid, acetic acid and lactic acid, other acids such as oxalic acid, butyric acid, pyruvic acid and gluconic acid have been used in the photo-assisted production of H₂ through the decarboxylation and photoreforming process. Acidic functionalities undergo decarboxylation into alkanes (for example, ethane, propane and butane). The photoreforming H₂ evolution increases with increases in the alkane chain length. H₂ fuel, also produced from fatty acids through steric acid as an intermediate, has been carried out using platinumized TiO₂ [141]. The oxidation of saccharides processed using biomass feedstocks results in forming acidic derivatives. Gluconic and threonine salts act as the substrate producing H₂ and CO₂ in the presence of Pt/TiO₂ in the presence of UV-rich light [60]. Yuexiang Li used oxalic acid as a sacrificial agent on Pt/TiO₂ in photoreforming, which produced H₂ and CO₂ in 1:2 molar ratio [72]. There are many reports on the use of different acids as sacrificial agents in photoreforming for the production of H₂, and other organic carboxylic acids are described in Table 4.

Table 4. Various catalysts, light sources and co-catalyst used in photoreforming of other carboxylic acids and the rate of hydrogen production.

Acid Concentration	Light Source, Wavelength (nm)	Photocatalyst	Co-Catalyst	Time Course (h)	Rate of Production ($\mu\text{molg}^{-1} \text{h}^{-1}$)			Reference
					H ₂	CO ₂	C ₂ H ₆	
<i>aq</i> , 0.01 M HOOC-COOH (Oxalic acid), pH 2	Hg	0.5%- Pt/P ₂₅ TiO ₂	Pt	5	2850	-	-	[72]
<i>aq</i> , 0.049 M HOOC-COOH (Oxalic acid)	Hg	0.5%- Pt/P ₂₅ TiO ₂	Pt	5	1160	-	-	[71]
<i>aq</i> , 0.001 M HOOC-COOH (Oxalic acid)	Hg	0.3%- Pt/P ₂₅ TiO ₂	Pt	5.5	3750	-	-	[142]
<i>aq</i> , 1.3 g/L HOCH ₂ (CHOH) ₄ COOH (Gluconic acid)	Hg	2%-Pt/TiO ₂	Pt	30	675	296	-	[141]
<i>aq</i> , 0.51 g/L H ₂ O/HOCH ₂ COOH (Glycolic acid)	Hg	2%-Pt/TiO ₂	Pt	46	284	109	-	[141]
H ₂ O/HOCH ₂ COOH (Glycolic acid) (1:10 v/v)	Xe, 360–520	5%- Pt/TiO ₂ (rutile)	Pt	5	105	76	-	[120]
H ₂ O/HOCH ₂ COOH (Glycolic acid) (1:10)	Xe	5%-Pt/CdS	Pt	5	392	3	-	[120]

Table 4. Cont.

Acid Concentration	Light Source, Wavelength (nm)	Photocatalyst	Co-Catalyst	Time Course (h)	Rate of Production ($\mu\text{mol g}^{-1} \text{ h}^{-1}$)			Reference
					H ₂	CO ₂	C ₂ H ₆	
<i>aq</i> , C ₁₈ H ₃₆ O ₂ or CH ₃ (CH ₂) ₁₆ COOH (Stearic acid) (1.7% <i>w/v</i>)	Xe	5%-Pt/TiO ₂	Pt	24	29	0	-	[60]
<i>aq</i> , H ₂ O/CH ₃ CH ₂ COOH (Propionic acid) (6:1)	Hg, 320	7%-Pt/TiO ₂ (rutile)	Pt		51	-	490	[111]
<i>aq</i> , H ₂ O/CH ₃ CH ₂ CH ₂ COOH (L-Propionic acid) (6:1)	Hg, 320	7%-Pt/TiO ₂ (rutile)	Pt		111	-	332	[111]
<i>aq</i> , H ₂ O/CH ₃ (CH ₂) ₃ COOH (6:1)	Hg	7%-Pt/TiO ₂ (rutile)	Pt		174	-	339	[111]
<i>l</i> , 6.66 g/L CH ₃ CH ₂ COOH (Butyric acid)	Hg, 420	1%-Pt/TiO ₂	Pt	>16	6800 ($\mu\text{mol h}^{-1}$)	-	-	[143]
<i>aq</i> , 5 mM CH ₃ CH ₂ CH ₂ COOH (Valeric acid) (400 °C)	LED, 360–370	Pt/TiO ₂ -NTs	Pt	8	387.5	362.5	-	[144]

5. Future Aspects

To gain a high rate and quantity of hydrogen evolution from various biomasses and organic molecules through photoreforming, the evolution of hydrogen (half-reaction) must be carefully enhanced by controlling the selectivity of the photoreforming of organic compounds into hydrogen and preventing the production of harmful organic waste products and also the development of value-added products. Subsequently, most researchers have focused on enhancing the rate and efficiency of selective hydrogen production through photoreforming. Various approaches are described in Figure 7, regarding catalyst design, the selection of co-catalysts, reaction media, advanced characterization and computational studies. The designing of photocatalysts is the most challenging field. Most researchers are moving towards using environment-friendly and cost-effective semiconducting material by synthesizing composites with various co-catalysts. The selection of cocatalysts must be made using earth-abundant, non-toxic and environment-friendly materials instead of precious and toxic metals (Pt, Ru, Ag and Pd). Most of the above-mentioned photocatalysts exhibit reasonable efficiency of organic acid conversion into H₂ and valuable products, but depth of the understanding of the mechanism, advanced characterization and computational studies are required to make use of photoreforming on an industrial scale and for commercialization. The photoreforming process of the conversion of organics into hydrogen fuel must be benign with a cost-effective photocatalyst, selectivity and efficiency.

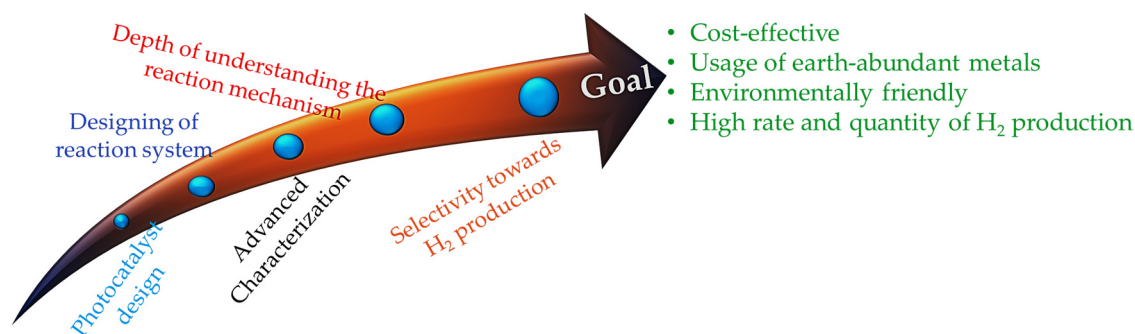


Figure 7. A proposed approach for the selective photoreforming of various acids into H₂ and valuable organic compounds.

6. Conclusions

In summary, the photocatalytic method has become the most challenging technique for renewable, zero-emission energy harvesting in the last few decades. The scientific community has shown excessive interest in employing photoactive materials and various reaction parameters for clean H₂ production using solar energy through water splitting and the photoreforming of organic molecules. When employing the right catalyst, sacrificial agent and solar energy to produce H₂, the organic process has been shown to be more advantageous and to have more industrial uses than the traditional water splitting method. The main challenge in photoreforming is developing an efficient, stable photocatalyst that can absorb sunlight. Along with this, important issues must be overcome, such as the development of co-catalysts without using noble, precious metals. Cost-effective, environmentally benign and abundant metals must be used as cocatalysts for commercialization and practical application. Recently, researchers have developed novel nanostructures with controlled morphology at the nanoscale and with multiphase composition. In addition, more attention should be given to addressing specific issues such as the reversible recombination of charges, and catalytic materials should be beneficial for H₂ photoproduction, therefore contributing to the appearance of great promise in this field. The combination of two or more materials can be performed towards optimizing photocatalytic activity. The choice of the proper material and understanding the mechanism of the catalyst material is needed, but it is still challenging in some reactions. There are various semiconductors developed with optimized band energy gaps and co-catalysts with photoactivity to produce hydrogen from oxygenated organics. Various organics are reformed into renewable sources and valuable hydrocarbons using UV-vis radiation and semiconducting materials. The catalyst is developed from bare TiO₂, a noble metal (Pt, Ru, Pd and Au) and TiO₂ to a transition metal and less toxic and cost-effective cocatalysts loaded with TiO₂ for carboxylic acid reforming. Furthermore, CdS and ZnS are used as semiconducting materials loaded with MoS₂ and Cu₂O for the formation of hydrogen from various carboxylic acids. The photocatalytic conversion of carboxylic acids occurs by decarboxylation and reforming into H₂, carbon monoxide, carbon dioxide and hydrocarbons. Overall, the critical factors for the efficiency of photoreforming are selectivity towards the high rate and quantity of hydrogen evolution, efficiency, sustainability and long-term chemical and photocatalytic stability, and reaction conditions with cost-effective, environmentally benign and easily available photocatalysts should be developed for carboxylic acid photoreforming.

Author Contributions: A.S. (Apurba Sinhamahapatra) and S.K.N. conceived the idea and finalized the manuscript. A.S. (Anita Samage), P.G. and M.A.H. performed the literature search and drafting. All authors have read and agreed to the published version of the manuscript.

Funding: S.K.N. would like to thank the Department of Science and Technology (Government of India) for the NANO MISSION Project (SR/NM/NT-1073/2016) and DST INSPIRE (IFA12-CH-84) and the DST-Technology Mission Division (DST/TMD/HFC/2K18/124G) (Government of India) for its economic support. S.K.N. acknowledges the “Talent Attraction Programme funded by the Community of Madrid Spain/Spanish (2017-T1/AMB5610)”. A.S. (Apurba Sinhamahapatra) acknowledges the research funds from the Department of Science and Technology (Government of India) for the DST INSPIRE Fellowship (IFA17-MS107).

Institutional Review Board Statement: Not applicable.

Informed Consent Statement: Not applicable.

Data Availability Statement: Not applicable.

Conflicts of Interest: The authors declare no conflict of interest.

References

1. Balali, Y.; Stegen, S. Review of energy storage systems for vehicles based on technology, environmental impacts, and costs. *Renew. Sustain. Energy Rev.* **2021**, *135*, 110185. [[CrossRef](#)]
2. Bhuiyan, M.A.; Khan, H.U.R.; Zaman, K.; Hishan, S.S. Measuring the impact of global tropospheric ozone, carbon dioxide and sulfur dioxide concentrations on biodiversity loss. *Environ. Res.* **2018**, *160*, 398–411. [[CrossRef](#)] [[PubMed](#)]
3. Blanco, H.; Nijs, W.; Ruf, J.; Faaij, A. Potential for hydrogen and Power-to-Liquid in a low-carbon EU energy system using cost optimization. *Appl. Energy* **2018**, *232*, 617–639. [[CrossRef](#)]
4. Chen, J.; Wang, Q.; Xu, Z.; Jiaqiang, E.; Leng, E.; Zhang, F.; Liao, G. Process in supercritical water gasification of coal: A review of fundamentals, mechanisms, catalysts and element transformation. *Energ. Convers. Manag.* **2021**, *237*, 114122. [[CrossRef](#)]
5. Chen, C.; Wood, P. A turbulence closure model for dilute gas-particle flows. *Can. J. Chem. Eng.* **1985**, *63*, 349–360. [[CrossRef](#)]
6. Nguyen, H.M.; Sunarso, J.; Li, C.; Pham, G.H.; Phan, C.; Liu, S. Microwave-assisted catalytic methane reforming: A review. *Appl. Catal. A. Gen.* **2020**, *599*, 117620. [[CrossRef](#)]
7. Ahmadi, M.H.; Ghazvini, M.; Alhuyi Nazari, M.; Ahmadi, M.A.; Pourfayaz, F.; Lorenzini, G.; Ming, T. Renewable energy harvesting with the application of nanotechnology: A review. *Int. J. Energy Res.* **2019**, *43*, 1387–1410. [[CrossRef](#)]
8. Luo, P. perspectives in photo-and electrochemical-oxidation of biomass for sustainable chemicals and hydrogen production. *Adv. Energy Mater* **2021**, *11*, 2101180. [[CrossRef](#)]
9. Luo, H.; Zeng, Z.; Zeng, G.; Zhang, C.; Xiao, R.; Huang, D.; Lai, C.; Cheng, M.; Wang, W.; Xiong, W. Recent progress on metal-organic frameworks based-and derived-photocatalysts for water splitting. *Chem. Eng. J.* **2020**, *383*, 123196. [[CrossRef](#)]
10. O'regan, B.; Grätzel, M. A low-cost, high-efficiency solar cell based on dye-sensitized colloidal TiO₂ films. *Nature* **1991**, *353*, 737–740. [[CrossRef](#)]
11. Navarro, R.M.; Sanchez-Sanchez, M.C.; Alvarez-Galvan, M.C.; Valle, F.; Fierro, J.L. Hydrogen production from renewable sources: Biomass and photocatalytic opportunities. *Energy Environ. Science.* **2009**, *2*, 35–54. [[CrossRef](#)]
12. Colmenares, J.C.; Magdziarz, A.; Aramendia, M.A.; Marinas, A.; Marinas, J.M.; Urbano, F.J.; Navio, J.A. Influence of the strong metal support interaction effect (SMSI) of Pt/TiO₂ and Pd/TiO₂ systems in the photocatalytic biohydrogen production from glucose solution. *Catal. Commun.* **2011**, *16*, 1–6. [[CrossRef](#)]
13. Bowker, M. Sustainable hydrogen production by the application of ambient temperature photocatalysis. *Green Chem.* **2011**, *13*, 2235–2246. [[CrossRef](#)]
14. Ran, J.; Gao, G.; Li, F.-T.; Ma, T.-Y.; Du, A.; Qiao, S.-Z. Ti₃C₂ MXene co-catalyst on metal sulfide photo-absorbers for enhanced visible-light photocatalytic hydrogen production. *Nat. Commun.* **2017**, *8*, 1–10. [[CrossRef](#)] [[PubMed](#)]
15. Lakhera, S.K.; Rajan, A.; Rugma, T.; Bernaurdshaw, N. A review on particulate photocatalytic hydrogen production system: Progress made in achieving high energy conversion efficiency and key challenges ahead. *Renew. Sustain. Energy Rev.* **2021**, *152*, 111694. [[CrossRef](#)]
16. Arkhipova, N.; Kuznetsova, A. Photocatalytic activity and physicochemical characteristics of modified potassium polytitanates in the reaction of decomposition of aqueous-alcoholic solutions. *Russ. J. Appl. Chem.* **2017**, *90*, 186–192. [[CrossRef](#)]
17. Patsoura, A.; Kondarides, D.I.; Verykios, X.E. Photocatalytic degradation of organic pollutants with simultaneous production of hydrogen. *Catal. Today.* **2007**, *124*, 94–102. [[CrossRef](#)]
18. Christoforidis, K.; Fornasiero, P. Photocatalytic hydrogen production: A rift into the future energy supply. *ChemCatChem* **2017**, *9*, 1523–1544. [[CrossRef](#)]
19. Colmenares, J.C.; Luque, R. Heterogeneous photocatalytic nanomaterials: Prospects and challenges in selective transformations of biomass-derived compounds. *Chem. Soc. Rev.* **2014**, *43*, 765–778. [[CrossRef](#)]
20. Quispe, C.A.; Coronado, C.J.; Carvalho, J.A., Jr. Glycerol: Production, consumption, prices, characterization and new trends in combustion. *Renew. Sustain. Energy Rev.* **2013**, *27*, 475–493. [[CrossRef](#)]
21. Pagliaro, M.; Ciriminna, R.; Kimura, H.; Rossi, M.; Della Pina, C. From glycerol to value-added products. *Angew. Chem. Int. Edition* **2007**, *46*, 4434–4440. [[CrossRef](#)] [[PubMed](#)]
22. Toe, C.Y.; Tsounis, C.; Zhang, J.; Masood, H.; Gunawan, D.; Scott, J.; Amal, R. Advancing photoreforming of organics: Highlights on photocatalyst and system designs for selective oxidation reactions. *Energy Environ. Sci.* **2021**, *14*, 1140–1175. [[CrossRef](#)]
23. Sinhamahapatra, A.; Jeon, J.-P.; Yu, J.-S. A new approach to prepare highly active and stable black titania for visible light-assisted hydrogen production. *Energy Environ. Sci.* **2015**, *8*, 3539–3544. [[CrossRef](#)]
24. McKone, J.R.; Pieterick, A.P.; Gray, H.B.; Lewis, N.S. Hydrogen evolution from Pt/Ru-coated p-type WSe₂ photocathodes. *J. Am. Chem. Soc.* **2013**, *135*, 223–231. [[CrossRef](#)] [[PubMed](#)]
25. Walte, M.; Warren, E.; McKone, J.; Boettcher, S.; Qixi, M.; Santori, E.; Lewis, N. Solar water splitting cell. *Chem. Rev.* **2010**, *110*, 6446–6473. [[CrossRef](#)] [[PubMed](#)]
26. Rossetti, I. Hydrogen production by photoreforming of renewable substrates. *Int. Sch. Res. Notices* **2012**, *2012*. [[CrossRef](#)]
27. Asahi, R.; Morikawa, T.; Ohwaki, T.; Aoki, K.; Taga, Y. Visible-light photocatalysis in nitrogen-doped titanium oxides. *Science* **2001**, *293*, 269–271. [[CrossRef](#)]
28. Khan, K.; Tareen, A.K.; Aslam, M.; Sagar, R.U.R.; Zhang, B.; Huang, W.; Mahmood, A.; Mahmood, N.; Khan, K.; Zhang, H. Recent progress, challenges, and prospects in two-dimensional photocatalyst materials and environmental remediation. *Micro Nano Lett.* **2020**, *12*, 1–77. [[CrossRef](#)]

29. Kawai, T.; Sakata, T. Conversion of carbohydrate into hydrogen fuel by a photocatalytic process. *Nature* **1980**, *286*, 474–476. [[CrossRef](#)]
30. Sakata, T.; Hashimoto, K.; Kawai, T. Catalytic properties of ruthenium oxide on n-type semiconductors under illumination. *J. Phys. Chem. A* **1984**, *88*, 5214–5221. [[CrossRef](#)]
31. Pajares, A.; Wang, Y.; Kronenberg, M.; de la Piscina, P.R.; Homs, N. Photocatalytic H₂ production from ethanol aqueous solution using TiO₂ with tungsten carbide nanoparticles as co-catalyst. *Int. J. Hydrogen Energy* **2020**, *45*, 20558–20567. [[CrossRef](#)]
32. Alshehri, A.; Narasimharao, K. PtOx-TiO₂ anatase nanomaterials for photocatalytic reformation of methanol to hydrogen: Effect of TiO₂ morphology. *J. Mater. Res. Technol.* **2020**, *9*, 14907–14921. [[CrossRef](#)]
33. Hippargi, G.; Anjankar, S.; Krupadam, R.J.; Rayalu, S.S. Simultaneous wastewater treatment and generation of blended fuel methane and hydrogen using Au-Pt/TiO₂ photo-reforming catalytic material. *Fuel* **2021**, *291*, 120113. [[CrossRef](#)]
34. Huang, C.-W.; Nguyen, B.-S.; Wu, J.C.-S.; Nguyen, V.-H. A current perspective for photocatalysis towards the hydrogen production from biomass-derived organic substances and water. *Int. J. Hydrogen Energy* **2020**, *45*, 18144–18159. [[CrossRef](#)]
35. Kumaravel, V.; Imam, M.D.; Badreldin, A.; Chava, R.K.; Do, J.Y.; Kang, M.; Abdel-Wahab, A. Photocatalytic hydrogen production: Role of sacrificial reagents on the activity of oxide, carbon, and sulfide catalysts. *Catalysts* **2019**, *9*, 276. [[CrossRef](#)]
36. Guzman, F.; Chuang, S.S.; Yang, C. Role of methanol sacrificing reagent in the photocatalytic evolution of hydrogen. *Ind. Eng. Chem. Res.* **2013**, *52*, 61–65. [[CrossRef](#)]
37. Ismael, M. Latest progress on the key operating parameters affecting the photocatalytic activity of TiO₂-based photocatalysts for hydrogen fuel production: A comprehensive review. *Fuel* **2021**, *303*, 121207. [[CrossRef](#)]
38. Li, Y.; Wang, B.; Liu, S.; Duan, X.; Hu, Z. Synthesis and characterization of Cu₂O/TiO₂ photocatalysts for H₂ evolution from aqueous solution with different scavengers. *Appl. Surf. Sci.* **2015**, *324*, 736–744. [[CrossRef](#)]
39. Chiarello, G.L.; Forni, L.; Selli, E. Photocatalytic hydrogen production by liquid-and-gas-phase reforming of CH₃OH over flame-made TiO₂ and Au/TiO₂. *Catal. Today* **2009**, *144*, 69–74. [[CrossRef](#)]
40. Vitiello, G.; Clarizia, L.; Abdelraheem, W.; Esposito, S.; Bonelli, B.; Ditaranto, N.; Vergara, A.; Nadagouda, M.; Dionysiou, D.D.; Andreozzi, R. Near UV-Irradiation of CuOx-Impregnated TiO₂ Providing Active Species for H₂ Production Through Methanol Photoreforming. *ChemCatChem* **2019**, *11*, 4314–4326. [[CrossRef](#)]
41. Asencios, Y.J.; Machado, V.A. Photodegradation of Organic Pollutants in Seawater and Hydrogen Production via Methanol Photoreforming with Hydrated Niobium Pentoxide Catalysts. *Sustain. Chem.* **2022**, *3*, 172–191. [[CrossRef](#)]
42. Saha, A.; Sinhamahapatra, A.; Kang, T.-H.; Ghosh, S.C.; Yu, J.-S.; Panda, A.B. Hydrogenated MoS₂ QD-TiO₂ heterojunction mediated efficient solar hydrogen production. *Nanoscale* **2017**, *9*, 17029–17036. [[CrossRef](#)]
43. Sinhamahapatra, A.; Lee, H.-Y.; Shen, S.; Mao, S.S.; Yu, J.-S. H-doped TiO_{2-x} prepared with MgH₂ for highly efficient solar-driven hydrogen production. *Appl. Catal. B* **2018**, *237*, 613–621. [[CrossRef](#)]
44. Gomathisankar, P.; Hachisuka, K.; Katsumata, H.; Suzuki, T.; Funasaka, K.; Kaneco, S. Enhanced photocatalytic hydrogen production from aqueous methanol solution using ZnO with simultaneous photodeposition of Cu. *Int. J. Hydrogen Energy* **2013**, *38*, 11840–11846. [[CrossRef](#)]
45. Sinhamahapatra, A.; Jeon, J.-P.; Kang, J.; Han, B.; Yu, J.-S. Oxygen-deficient zirconia (ZrO_{2-x}): A new material for solar light absorption. *Sci. Rep.* **2016**, *6*, 1–8. [[CrossRef](#)] [[PubMed](#)]
46. Nguyen-Phan, T.-D.; Baber, A.E.; Rodriguez, J.A.; Senanayake, S.D. Au and Pt nanoparticle supported catalysts tailored for H₂ production: From models to powder catalysts. *Appl. Catal. A Gen.* **2016**, *518*, 18–47. [[CrossRef](#)]
47. Sampaio, M.J.; Oliveira, J.W.; Sombrio, C.I.; Baptista, D.L.; Teixeira, S.R.; Carabineiro, S.A.; Silva, C.G.; Faria, J.L. Photocatalytic performance of Au/ZnO nanocatalysts for hydrogen production from ethanol. *Appl. Catal. A Gen.* **2016**, *518*, 198–205. [[CrossRef](#)]
48. Montini, T.; Gombac, V.; Sordelli, L.; Delgado, J.J.; Chen, X.; Adami, G.; Fornasiero, P. Nanostructured Cu/TiO₂ Photocatalysts for H₂ Production from Ethanol and Glycerol Aqueous Solutions. *ChemCatChem* **2011**, *3*, 574–577. [[CrossRef](#)]
49. Zhang, X.; Luo, L.; Yun, R.; Pu, M.; Zhang, B.; Xiang, X. Increasing the activity and selectivity of TiO₂-supported Au catalysts for renewable hydrogen generation from ethanol photoreforming by engineering Ti³⁺ defects. *ACS Sustain. Chem. Eng.* **2019**, *7*, 13856–13864. [[CrossRef](#)]
50. Gunawan, D.; Toe, C.Y.; Kumar, P.; Scott, J.; Amal, R. Synergistic Cyanamide Functionalization and Charge-Induced Activation of Nickel/Carbon Nitride for Enhanced Selective Photoreforming of Ethanol. *ACS Appl. Mater. Interfaces* **2021**, *13*, 49916–49926. [[CrossRef](#)]
51. Tran, N.H.; Kannangara, G.K. Conversion of glycerol to hydrogen rich gas. *Chem. Soc. Rev.* **2013**, *42*, 9454–9479. [[CrossRef](#)] [[PubMed](#)]
52. Zhong, W.; Wang, C.; Zhao, H.; Peng, S.; Tian, Z.; Shu, R.; Chen, Y. Synergistic Effect of Photo-thermal Catalytic Glycerol Reforming Hydrogen Production over 2D Au/TiO₂ Nanoflakes. *Chem. Eng. J.* **2022**, 137063. [[CrossRef](#)]
53. Iervolino, G.; Vaiano, V.; Murcia, J.; Lara, A.; Hernández, J.; Rojas, H.; Navío, J.; Hidalgo, M. Photocatalytic production of hydrogen and methane from glycerol reforming over Pt/TiO₂-Nb₂O₅. *Int. J. Hydrogen Energy* **2021**, *46*, 38678–38691. [[CrossRef](#)]
54. Tahir, M.; Siraj, M.; Tahir, B.; Umer, M.; Alias, H.; Othman, N. Au-NPs embedded Z-scheme WO₃/TiO₂ nanocomposite for plasmon-assisted photocatalytic glycerol-water reforming towards enhanced H₂ evolution. *Appl. Surf. Sci.* **2020**, *503*, 144344. [[CrossRef](#)]
55. St. John, M.R.; Furgala, A.J.; Sammells, A.F. Hydrogen generation by photocatalytic oxidation of glucose by platinumized n-titania powder. *J. Phys. Chem. A* **1983**, *87*, 801–805. [[CrossRef](#)]

56. Fu, X.; Long, J.; Wang, X.; Leung, D.Y.; Ding, Z.; Wu, L.; Zhang, Z.; Li, Z.; Fu, X. Photocatalytic reforming of biomass: A systematic study of hydrogen evolution from glucose solution. *Int. J. Hydrogen Energy* **2008**, *33*, 6484–6491. [[CrossRef](#)]
57. Iervolino, G.; Vaiano, V.; Sannino, D.; Rizzo, L.; Ciambelli, P. Production of hydrogen from glucose by LaFeO₃ based photocatalytic process during water treatment. *Int. J. Hydrogen Energy* **2016**, *41*, 959–966. [[CrossRef](#)]
58. Nguyen, V.-C.; Nimbalkar, D.B.; Nam, L.D.; Lee, Y.-L.; Teng, H. Photocatalytic cellulose reforming for H₂ and formate production by using graphene oxide-dot catalysts. *ACS Catal.* **2021**, *11*, 4955–4967. [[CrossRef](#)]
59. Mondal, A.; Biswas, S.; Kumar, A.; Yu, J.S.; Sinhamahapatra, A. Sub 10 nm CoO nanoparticle-decorated graphitic carbon nitride for solar hydrogen generation via efficient charge separation. *Nanoscale Adv.* **2020**, *2*, 4473–4481. [[CrossRef](#)]
60. Kawai, T.; Sakata, T. Photocatalytic hydrogen production from water by the decomposition of poly-vinylchloride, protein, algae, dead insects, and excrement. *Chem. Lett.* **1981**, *10*, 81–84. [[CrossRef](#)]
61. Razzaq, A.; Sinhamahapatra, A.; Kang, T.-H.; Grimes, C.A.; Yu, J.-S.; In, S.-I. Efficient solar light photoreduction of CO₂ to hydrocarbon fuels via magnesiothermally reduced TiO₂ photocatalyst. *Appl. Catal. B* **2017**, *215*, 28–35. [[CrossRef](#)]
62. Greenbaum, E.; Tevault, C.V.; Ma, C. New Photosynthesis: Direct photoconversion of biomass to molecular oxygen and volatile hydrocarbons. *Energy Fuels* **1995**, *9*, 163–167. [[CrossRef](#)]
63. Wu, X.; Fan, X.; Xie, S.; Lin, J.; Cheng, J.; Zhang, Q.; Chen, L.; Wang, Y. Solar energy-driven lignin-first approach to full utilization of lignocellulosic biomass under mild conditions. *Nat. Catal.* **2018**, *1*, 772–780. [[CrossRef](#)]
64. Speltini, A.; Gualco, F.; Maraschi, F.; Sturini, M.; Dondi, D.; Malavasi, L.; Profumo, A. Photocatalytic hydrogen evolution assisted by aqueous (waste) biomass under simulated solar light: Oxidized g-C₃N₄ vs. P25 titanium dioxide. *Int. J. Hydrogen Energy* **2019**, *44*, 4072–4078. [[CrossRef](#)]
65. Liu, Q.; Wei, L.; Xi, Q.; Lei, Y.; Wang, F. Edge functionalization of terminal amino group in carbon nitride by in-situ C–N coupling for photoreforming of biomass into H₂. *Chem. Eng. J.* **2020**, *383*, 123792. [[CrossRef](#)]
66. Guo, P.; Xiong, Z.; Yuan, S.; Xie, K.; Wang, H.; Gao, Y. The synergistic effect of Co/CoO hybrid structure combined with biomass materials promotes photocatalytic hydrogen evolution. *Chem. Eng. J.* **2021**, *420*, 130372. [[CrossRef](#)]
67. Yasuda, M.; Matsumoto, T.; Yamashita, T. Sacrificial hydrogen production over TiO₂-based photocatalysts: Polyols, carboxylic acids, and saccharides. *Renew. Sustain. Energy Rev.* **2018**, *81*, 1627–1635. [[CrossRef](#)]
68. Tan, H.; Kong, P.; Liu, M.; Gu, X.; Zheng, Z. Enhanced photocatalytic hydrogen production from aqueous-phase methanol reforming over cyano-carboxylic bifunctionally-modified carbon nitride. *ChemComm.* **2019**, *55*, 12503–12506. [[CrossRef](#)]
69. Liu, X.; Duan, X.; Wei, W.; Wang, S.; Ni, B.-J. Photocatalytic conversion of lignocellulosic biomass to valuable products. *Green Chem.* **2019**, *21*, 4266–4289. [[CrossRef](#)]
70. AlSalka, Y.; Al-Madanat, O.; Curti, M.; Hakki, A.; Bahnemann, D.W. Photocatalytic H₂ evolution from oxalic acid: Effect of cocatalysts and carbon dioxide radical anion on the surface charge transfer mechanisms. *ACS Appl. Energy Mater.* **2020**, *3*, 6678–6691. [[CrossRef](#)]
71. Li, Y.; Lu, G.; Li, S. Photocatalytic hydrogen generation and decomposition of oxalic acid over platinumized TiO₂. *Appl. Catal. A Gen.* **2001**, *214*, 179–185. [[CrossRef](#)]
72. Li, Y.; Lu, G.; Li, S. Photocatalytic production of hydrogen in single component and mixture systems of electron donors and monitoring adsorption of donors by in situ infrared spectroscopy. *Chemosphere* **2003**, *52*, 843–850. [[CrossRef](#)]
73. Zielińska, B.; Borowiak-Palen, E.; Kalenczuk, R.J. Photocatalytic hydrogen generation over alkaline-earth titanates in the presence of electron donors. *Int. J. Hydrogen Energy* **2008**, *33*, 1797–1802. [[CrossRef](#)]
74. Reuss, G.; Disteldorf, W.; Grundler, O.; Hilt, A. *Ullmann's Encycl*; Society of Chemical Industry: Chichester, UK, 1985.
75. Klankermayer, J.; Wesselbaum, S.; Beydoun, K.; Leitner, W. Cover Picture: Selective Catalytic Synthesis Using the Combination of Carbon Dioxide and Hydrogen: Catalytic Chess at the Interface of Energy and Chemistry (Angew. Chem. Int. Ed. 26/2016). *Angew. Chem. Int. Ed.* **2016**, *55*, 7267. [[CrossRef](#)]
76. Tao, C.; Guopeng, W.; Zhaochi, F.; Gengshen, H.; Weiguang, S.; Pinliang, Y.; Can, L. In situ FT-IR study of photocatalytic decomposition of formic acid to hydrogen on Pt/TiO₂ catalyst. *Chin. J. Catal.* **2008**, *29*, 105–107.
77. Lanese, V.; Spasiano, D.; Marotta, R.; Di Somma, I.; Lisi, L.; Cimino, S.; Andreozzi, R. Hydrogen production by photoreforming of formic acid in aqueous copper/TiO₂ suspensions under UV-simulated solar radiation at room temperature. *Int. J. Hydrogen Energy* **2013**, *38*, 9644–9654.
78. Hainer, A.S.; Hodgins, J.S.; Sandre, V.; Vallieres, M.; Lanterna, A.E.; Scaiano, J.C. Photocatalytic hydrogen generation using metal-decorated TiO₂: Sacrificial donors vs. true water splitting. *ACS Energy Lett.* **2018**, *3*, 542–545.
79. Nasir, J.A.; Hafeez, M.; Arshad, M.; Ali, N.Z.; Teixeira, I.F.; McPherson, I.; Khan, M.A. Photocatalytic dehydrogenation of formic acid on CdS nanorods through Ni and Co redox mediation under mild conditions. *ChemSusChem* **2018**, *11*, 2587–2592. [[CrossRef](#)]
80. Chiarello, G.L.; Aguirre, M.H.; Selli, E. Hydrogen production by photocatalytic steam reforming of methanol on noble metal-modified TiO₂. *J. Catal.* **2010**, *273*, 182–190. [[CrossRef](#)]
81. Song, R.; Luo, B.; Liu, M.; Geng, J.; Jing, D.; Liu, H. Synergetic coupling of photo and thermal energy for efficient hydrogen production by formic acid reforming. *AIChE J.* **2017**, *63*, 2916–2925. [[CrossRef](#)]
82. Willner, I.; Goren, Z. Photodecomposition of formic acid by cadmium sulphide semiconductor particles. *J. Chem. Soc. Chem. Commun.* **1986**, *2*, 172–173. [[CrossRef](#)]
83. Li, Y.; Du, J.; Peng, S.; Xie, D.; Lu, G.; Li, S. Enhancement of photocatalytic activity of cadmium sulfide for hydrogen evolution by photoetching. *Int. J. Hydrogen Energy.* **2008**, *33*, 2007–2013. [[CrossRef](#)]

84. Li, Y.; Hu, Y.; Peng, S.; Lu, G.; Li, S. Synthesis of CdS nanorods by an ethylenediamine assisted hydrothermal method for photocatalytic hydrogen evolution. *J. Phys. Chem. A C* **2009**, *113*, 9352–9358. [[CrossRef](#)]
85. Matsumura, M.; Hiramoto, M.; Iehara, T.; Tsubomura, H. Photocatalytic and photoelectrochemical reactions of aqueous solutions of formic acid, formaldehyde, and methanol on platinized cadmium sulfide powder and at a cadmium sulfide electrode. *J. Phys. Chem. A* **1984**, *88*, 248–250. [[CrossRef](#)]
86. Zhang, Z.; Cao, S.-W.; Liao, Y.; Xue, C. Selective photocatalytic decomposition of formic acid over AuPd nanoparticle-decorated TiO₂ nanofibers toward high-yield hydrogen production. *Appl. Catal. B* **2015**, *162*, 204–209. [[CrossRef](#)]
87. Puangpetch, T.; Chavadej, S.; Sreethawong, T. Hydrogen production over Au-loaded mesoporous-assembled SrTiO₃ nanocrystal photocatalyst: Effects of molecular structure and chemical properties of hole scavengers. *Energy Convers. Manag.* **2011**, *52*, 2256–2261. [[CrossRef](#)]
88. Zhu, R.; Tian, F.; Yang, R.; He, J.; Zhong, J.; Chen, B. Z scheme system ZnIn₂S₄/RGO/BiVO₄ for hydrogen generation from water splitting and simultaneous degradation of organic pollutants under visible light. *Renew. Energy* **2019**, *139*, 22–27. [[CrossRef](#)]
89. Wu, G.; Chen, T.; Su, W.; Zhou, G.; Zong, X.; Lei, Z.; Li, C. H₂ production with ultra-low CO selectivity via photocatalytic reforming of methanol on Au/TiO₂ catalyst. *Int. J. Hydrogen Energy* **2008**, *33*, 1243–1251. [[CrossRef](#)]
90. Zhang, Y.J.; Zhang, L. Photocatalytic degradation of formic acid with simultaneous production of hydrogen over Pt and Ru-loaded CdS/Al-HMS photocatalysts. *Desalination* **2009**, *249*, 1017–1021. [[CrossRef](#)]
91. Zhang, Y.J.; Zhang, L.; Li, S. Synthesis of Al-substituted mesoporous silica coupled with CdS nanoparticles for photocatalytic generation of hydrogen. *Int. J. Hydrogen Energy* **2010**, *35*, 438–444. [[CrossRef](#)]
92. Kuehnel, M.F.; Wakerley, D.W.; Orchard, K.L.; Reisner, E. Photocatalytic formic acid conversion on CdS nanocrystals with controllable selectivity for H₂ or CO. *Angew. Chem. Int. Ed.* **2015**, *54*, 9627–9631. [[CrossRef](#)] [[PubMed](#)]
93. Yeh, H.; Lo, S.; Chen, M.; Chen, H. Hydrogen production from formic acid solution by modified TiO₂ and titanate nanotubes in a two-step system under visible light irradiation. *Water Sci. Technol.* **2014**, *69*, 1676–1681. [[CrossRef](#)] [[PubMed](#)]
94. Chen, H.-Y.; Lo, S.-L.; Lai, Y.-C.; Liou, Y.-H. Titanate nanotubes coupled with Pt nanoparticles for the inhibition of CdS photocorrosion during visible-light-driven hydrogen production from formic acid. *Mater. Res. Express.* **2018**, *5*, 095507. [[CrossRef](#)]
95. Li, Y.; Tang, L.; Peng, S.; Li, Z.; Lu, G. Phosphate-assisted hydrothermal synthesis of hexagonal CdS for efficient photocatalytic hydrogen evolution. *CrystEngComm* **2012**, *14*, 6974–6982.
96. Cai, Y.; Li, X.; Zhang, Y.; Wei, X.; Wang, K.; Chen, J. Highly Efficient Dehydrogenation of Formic Acid over a Palladium-Nanoparticle-Based Mott-Schottky Photocatalyst. *Angew. Chem.* **2013**, *125*, 12038–12041. [[CrossRef](#)]
97. Kakuta, S.; Abe, T. A novel example of molecular hydrogen generation from formic acid at visible-light-responsive photocatalyst. *ACS Appl. Mater. Interfaces* **2009**, *1*, 2707–2710. [[CrossRef](#)] [[PubMed](#)]
98. Loges, B.; Boddien, A.; Gärtner, F.; Junge, H.; Beller, M. Catalytic generation of hydrogen from formic acid and its derivatives: Useful hydrogen storage materials. *Top. Catal.* **2010**, *53*, 902–914.
99. Park, J.Y.; Lee, I.H. Decomposition of acetic acid by advanced oxidation processes. *Korean J. Chem Eng.* **2009**, *26*, 387–391.
100. Hisatomi, T.; Kubota, J.; Domen, K. Recent advances in semiconductors for photocatalytic and photoelectrochemical water splitting. *Chem. Soc. Rev.* **2014**, *43*, 7520–7535. [[CrossRef](#)]
101. Kraeutler, B.; Bard, A.J. Heterogeneous photocatalytic decomposition of saturated carboxylic acids on titanium dioxide powder. *Decarboxylative Route Alkanes. J. Am. Chem. Soc.* **1978**, *100*, 5985–5992.
102. Yoneyama, H.; Takao, Y.; Tamura, H.; Bard, A.J. Factors influencing product distribution in photocatalytic decomposition of aqueous acetic acid on platinized titania. *J. Phys. Chem. A* **1983**, *87*, 1417–1422. [[CrossRef](#)]
103. Zheng, X.-J.; Wei, L.-F.; Zhang, Z.-H.; Jiang, Q.-J.; Wei, Y.-J.; Xie, B.; Wei, M.-B. Research on photocatalytic H₂ production from acetic acid solution by Pt/TiO₂ nanoparticles under UV irradiation. *Int. J. Hydrogen Energy* **2009**, *34*, 9033–9041. [[CrossRef](#)]
104. Zheng, X.-J.; Wei, Y.-J.; Wei, L.-F.; Xie, B.; Wei, M.-B. Photocatalytic H₂ production from acetic acid solution over CuO/SnO₂ nanocomposites under UV irradiation. *Int. J. Hydrogen Energy* **2010**, *35*, 11709–11718. [[CrossRef](#)]
105. Imizcoz, M.; Puga, A.V. Optimising hydrogen production via solar acetic acid photoreforming on Cu/TiO₂. *Catal. Sci. Technol.* **2019**, *9*, 1098–1102. [[CrossRef](#)]
106. Asal, S.; Saif, M.; Hafez, H.; Mozia, S.; Heciak, A.; Moszyński, D.; Abdel-Mottaleb, M. Photocatalytic generation of useful hydrocarbons and hydrogen from acetic acid in the presence of lanthanide modified TiO₂. *Int. J. Hydrogen Energy* **2011**, *36*, 6529–6537. [[CrossRef](#)]
107. Sun, W.; Zhang, S.; Liu, Z.; Wang, C.; Mao, Z. Studies on the enhanced photocatalytic hydrogen evolution over Pt/PEG-modified TiO₂ photocatalysts. *Int. J. Hydrogen Energy* **2008**, *33*, 1112–1117. [[CrossRef](#)]
108. Sreethawong, T.; Puangpetch, T.; Chavadej, S.; Yoshikawa, S. Quantifying influence of operational parameters on photocatalytic H₂ evolution over Pt-loaded nanocrystalline mesoporous TiO₂ prepared by single-step sol-gel process with surfactant template. *J. Power Sources* **2007**, *165*, 861–869. [[CrossRef](#)]
109. Hamid, S.; Ivanova, I.; Jeon, T.H.; Dillert, R.; Choi, W.; Bahnemann, D.W. Photocatalytic conversion of acetate into molecular hydrogen and hydrocarbons over Pt/TiO₂: pH dependent formation of Kolbe and Hofer-Moest products. *J. Catal.* **2017**, *349*, 128–135. [[CrossRef](#)]
110. Sato, S. Photo-Kolbe reaction at gas-solid interfaces. *J. Phys. Chem. A* **1983**, *87*, 3531–3537. [[CrossRef](#)]
111. Sakata, T.; Kawai, T.; Hashimoto, K. Heterogeneous photocatalytic reactions of organic acids and water. New React. Paths Besides Photo-Kolbe React. *J. Phys. Chem. A* **1984**, *88*, 2344–2350. [[CrossRef](#)]

112. Heciak, A.; Morawski, A.W.; Grzmil, B.; Mozia, S. Cu-modified TiO₂ photocatalysts for decomposition of acetic acid with simultaneous formation of C1–C3 hydrocarbons and hydrogen. *Appl. Catal. B* **2013**, *140*, 108–114. [[CrossRef](#)]
113. Mozia, S.; Heciak, A.; Morawski, A.W. Preparation of Fe-modified photocatalysts and their application for generation of useful hydrocarbons during photocatalytic decomposition of acetic acid. *J. Photochem. Photobiol.* **2010**, *216*, 275–282. [[CrossRef](#)]
114. Mozia, S.; Heciak, A.; Morawski, A.W. Photocatalytic acetic acid decomposition leading to the production of hydrocarbons and hydrogen on Fe-modified TiO₂. *Catal. Today* **2011**, *161*, 189–195. [[CrossRef](#)]
115. Sclafani, A.; Palmisano, L.; Schiavello, M.; Augugliaro, V.; Coluccia, S.; Marchese, L. The photodecomposition of ethanoic acid adsorbed over semiconductor and insulator oxides. *I. Pure Oxides. New J. Chem. (1987)* **1988**, *12*, 129–135.
116. Abdel-Rahman, M.A.; Tashiro, Y.; Sonomoto, K. Lactic acid production from lignocellulose-derived sugars using lactic acid bacteria: Overview and limits. *J. Biotechnol.* **2011**, *156*, 286–301. [[CrossRef](#)] [[PubMed](#)]
117. Joshi, D.; Singhvi, M.; Khire, J.; Gokhale, D. Strain improvement of *Lactobacillus lactis* for D-lactic acid production. *Biotechnol. Lett.* **2010**, *32*, 517–520. [[CrossRef](#)]
118. Zhang, W.; Wang, Y.; Wang, Z.; Zhong, Z.; Xu, R. Highly efficient and noble metal-free NiS/CdS photocatalysts for H₂ evolution from lactic acid sacrificial solution under visible light. *ChemComm* **2010**, *46*, 7631–7633. [[CrossRef](#)]
119. Harada, H.; Sakata, T.; Ueda, T. Effect of semiconductor on photocatalytic decomposition of lactic acid. *J. Am. Chem. Soc.* **1985**, *107*, 1773–1774. [[CrossRef](#)]
120. Harada, H.; Sakata, T.; Ueda, T. Semiconductor effect on the selective photocatalytic reaction of. *alpha.-hydroxycarboxylic acids. J. Phys. Chem. A* **1989**, *93*, 1542–1548.
121. Li, Q.; Guo, B.; Yu, J.; Ran, J.; Zhang, B.; Yan, H.; Gong, J.R. Highly efficient visible-light-driven photocatalytic hydrogen production of CdS-cluster-decorated graphene nanosheets. *J. Am. Chem. Soc.* **2011**, *133*, 10878–10884. [[CrossRef](#)]
122. Zong, X.; Han, J.; Ma, G.; Yan, H.; Wu, G.; Li, C. Photocatalytic H₂ evolution on CdS loaded with WS₂ as cocatalyst under visible light irradiation. *J. Phys. Chem. A C* **2011**, *115*, 12202–12208. [[CrossRef](#)]
123. Hu, Z.; Jimmy, C.Y. Pt 3 Co-loaded CdS and TiO₂ for photocatalytic hydrogen evolution from water. *J. Mater. Chem.* **2013**, *1*, 12221–12228. [[CrossRef](#)]
124. Li, C.; Wang, H.; Naghadeh, S.B.; Zhang, J.Z.; Fang, P. Visible light driven hydrogen evolution by photocatalytic reforming of lignin and lactic acid using one-dimensional NiS/CdS nanostructures. *Appl. Catal. B* **2018**, *227*, 229–239. [[CrossRef](#)]
125. Zong, X.; Yan, H.; Wu, G.; Ma, G.; Wen, F.; Wang, L.; Li, C. Enhancement of photocatalytic H₂ evolution on CdS by loading MoS₂ as cocatalyst under visible light irradiation. *J. Am. Chem. Soc.* **2008**, *130*, 7176–7177. [[CrossRef](#)]
126. Chen, G.; Li, D.; Li, F.; Fan, Y.; Zhao, H.; Luo, Y.; Yu, R.; Meng, Q. Ball-milling combined calcination synthesis of MoS₂/CdS photocatalysts for high photocatalytic H₂ evolution activity under visible light irradiation. *Appl. Catal. A Gen.* **2012**, *443*, 138–144. [[CrossRef](#)]
127. Lang, D.; Shen, T.; Xiang, Q. Roles of MoS₂ and graphene as cocatalysts in the enhanced visible-light photocatalytic H₂ production activity of multiarmed CdS nanorods. *ChemCatChem* **2015**, *7*, 943–951. [[CrossRef](#)]
128. Li, Y.; Wang, H.; Peng, S. Tunable photodeposition of MoS₂ onto a composite of reduced graphene oxide and CdS for synergic photocatalytic hydrogen generation. *J. Phys. Chem. A C* **2014**, *118*, 19842–19848. [[CrossRef](#)]
129. Chang, K.; Mei, Z.; Wang, T.; Kang, Q.; Ouyang, S.; Ye, J. MoS₂/graphene cocatalyst for efficient photocatalytic H₂ evolution under visible light irradiation. *ACS Nano* **2014**, *8*, 7078–7087. [[CrossRef](#)]
130. Shaislamov, U.; Yang, B.L. CdS-sensitized single-crystalline TiO₂ nanorods and polycrystalline nanotubes for solar hydrogen generation. *J. Mater. Res.* **2013**, *28*, 418–423. [[CrossRef](#)]
131. Hou, Y.; Laursen, A.B.; Zhang, J.; Zhang, G.; Zhu, Y.; Wang, X.; Dahl, S.; Chorkendorff, I. Layered nanojunctions for hydrogen-evolution catalysis. *Angew. Chem.* **2013**, *125*, 3709–3713. [[CrossRef](#)]
132. Pham, M.-H.; Dinh, C.-T.; Vuong, G.-T.; Ta, N.-D.; Do, T.-O. Visible light induced hydrogen generation using a hollow photocatalyst with two cocatalysts separated on two surface sides. *Phys. Chem. Chem. Phys.* **2014**, *16*, 5937–5941. [[CrossRef](#)] [[PubMed](#)]
133. Tu, H.; Xu, L.; Mou, F.; Guan, J. Single crystalline tantalum oxychloride microcubes: Controllable synthesis, formation mechanism and enhanced photocatalytic hydrogen production activity. *ChemComm* **2015**, *51*, 12455–12458. [[CrossRef](#)]
134. Cao, S.; Chen, Y.; Wang, C.-J.; Lv, X.-J.; Fu, W.-F. Spectacular photocatalytic hydrogen evolution using metal-phosphide/CdS hybrid catalysts under sunlight irradiation. *ChemComm* **2015**, *51*, 8708–8711. [[CrossRef](#)]
135. Cao, S.; Chen, Y.; Kang, L.; Lin, Z.; Fu, W.-F. Enhanced photocatalytic H₂-evolution by immobilizing CdS nanocrystals on ultrathin Co_{0.85}Se/RGO-PEI nanosheets. *J. Mater. Chem. A* **2015**, *3*, 18711–18717. [[CrossRef](#)]
136. Pan, Y.X.; Zhuang, H.; Hong, J.; Fang, Z.; Liu, H.; Liu, B.; Huang, Y.; Xu, R. Cadmium Sulfide Quantum Dots Supported on Gallium and Indium Oxide for Visible-Light-Driven Hydrogen Evolution from Water. *ChemSusChem* **2014**, *7*, 2537–2544. [[CrossRef](#)]
137. Wang, X.; Yu, H.; Yang, L.; Shao, L.; Xu, L. A highly efficient and noble metal-free photocatalytic system using Ni₃B/CdS as photocatalyst for visible light H₂ production from aqueous solution. *Catal. Commun.* **2015**, *67*, 45–48. [[CrossRef](#)]
138. Hu, J.; Liu, A.; Jin, H.; Ma, D.; Yin, D.; Ling, P.; Wang, S.; Lin, Z.; Wang, J. A versatile strategy for shish-kebab-like multi-heterostructured chalcogenides and enhanced photocatalytic hydrogen evolution. *J. Am. Chem. Soc.* **2015**, *137*, 11004–11010. [[CrossRef](#)]
139. Shen, L.; Luo, M.; Liu, Y.; Liang, R.; Jing, F.; Wu, L. Noble-metal-free MoS₂ co-catalyst decorated UiO-66/CdS hybrids for efficient photocatalytic H₂ production. *Appl. Catal. B Environ.* **2015**, *166*, 445–453. [[CrossRef](#)]

140. Liu, K.; Litke, A.; Su, Y.; Van Campenhout, B.G.; Pidko, E.A.; Hensen, E.J. Photocatalytic decarboxylation of lactic acid by Pt/TiO₂. *ChemComm* **2016**, *52*, 11634–11637. [[CrossRef](#)]
141. Shiragami, T.; Tomo, T.; Tsumagari, H.; Yuki, R.; Yamashita, T.; Yasuda, M. Pentose acting as a sacrificial multielectron source in photocatalytic hydrogen evolution from water by Pt-doped TiO₂. *Chem. Lett.* **2012**, *41*, 29–31. [[CrossRef](#)]
142. Li, Y.; Lu, G.; Li, S. Photocatalytic transformation of rhodamine B and its effect on hydrogen evolution over Pt/TiO₂ in the presence of electron donors. *J. Photochem. Photobiol.* **2002**, *152*, 219–228. [[CrossRef](#)]
143. Wei, L.F.; Zheng, X.J.; Zhang, Z.H.; Wei, Y.J.; Xie, B.; Wei, M.B.; Sun, X.L. A systematic study of photocatalytic H₂ production from propionic acid solution over Pt/TiO₂ photocatalyst. *Int. J. Energy Res.* **2012**, *36*, 75–86. [[CrossRef](#)]
144. Scandura, G.; Rodríguez, J.; Palmisano, G. Hydrogen and propane production from butyric acid photoreforming over Pt-TiO₂. *Front. Chem.* **2019**, *7*, 563. [[CrossRef](#)] [[PubMed](#)]